Computer Methods and Programs in Biomedicine 254 (2024) 108296

Contents lists available at ScienceDirect

Computer Methods and Programs in Biomedicine

journal homepage: https://www.sciencedirect.com/journal/computer-methods-and-programs-in-biomedicine

Impact of geometric and hemodynamic changes on a mechanobiological model of atherosclerosis

Patricia Hernández-López [a,*], Myriam Cilla [a,b], Miguel A. Martínez [a,b], Estefanía Peña [a,b], Mauro Malvè [b,c]

[a] Aragón Institute of Engineering Research (I3A), University of Zaragoza, Zaragoza, 50015, Spain
[b] Biomedical Research Networking Center in Bioengineering, Biomaterials and Nanomedicine (CIBER-BBN), Zaragoza, Spain
[c] Public University of Navarra (UPNA), Pamplona, Spain

ARTICLE INFO

Keywords:
Atherosclerosis
Carotid artery
2D-axisymmetric model
Three pore model
Double stenosis phenomenon
Geometry and hemodynamic changes

ABSTRACT

Background and Objective: In this work, the analysis of the importance of hemodynamic updates on a mechanobiological model of atheroma plaque formation is proposed.
Methods: For that, we use an idealized and axisymmetric model of carotid artery. In addition, the behavior of endothelial cells depending on hemodynamical changes is analyzed too. A total of three computational simulations are carried out and their results are compared: an uncoupled model and two models that consider the opposite behavior of endothelial cells caused by hemodynamic changes. The model considers transient blood flow using the Navier–Stokes equation. Plasma flow across the endothelium is determined with Darcy's law and the Kedem–Katchalsky equations, considering the three-pore model, which is also employed for the flow of substances across the endothelium. The behavior of the considered substances in the arterial wall is modeled with convection–diffusion–reaction equations, and the arterial wall is modeled as a hyperelastic Yeoh's material.
Results: Significant variations are noted in both the morphology and stenosis ratio of the plaques when comparing the uncoupled model to the two models incorporating updates for geometry and hemodynamic stimuli. Besides, the phenomenon of double-stenosis is naturally reproduced in the models that consider both geometric and hemodynamical changes due to plaque growth, whereas it cannot be predicted in the uncoupled model.
Conclusions: The findings indicate that integrating the plaque growth model with geometric and hemodynamic settings is essential in determining the ultimate shape and dimensions of the carotid plaque.

1. Introduction

Cardiovascular diseases are one of the main causes of mortality worldwide. Among these diseases, atherosclerosis, which is a pathology that causes an increase in the arterial wall thickness due to an accumulation of some substances in it (atheroma plaque), is the most common acquired vascular disease [1]. Atheroma plaques result, among others, in the narrowing of the arterial lumen and in a loss of arterial wall elasticity. In addition, atheroma plaques can break and lead to the formation of a thrombus. Therefore, it can derive into several events, such as heart attacks, ischaemias, or strokes [2].

There are many factors that contribute to the development of atherosclerosis, which can be categorized as systemic, biological and biomechanical. Systemic factors include high blood levels of low-density lipoproteins (LDL), hypertension and diabetes [3]. Biological factors include endothelial cell dysfunction, inflammation and genetic predisposition [4]. Biomechanical factors include hemodynamic forces such as shear stress, which can alter the shape and function of endothelial cells, and lesions of the arterial wall, which increase its permeability [5]. Although this pathology has been extensively studied, it is not yet fully understood. It is therefore essential to understand the process by which atheroma plaques form and how mechanical stimuli affect their growth and location. This understanding may help predict areas susceptible to plaque formation, allowing early detection, prevention or delay of plaque development.

Numerous studies have investigated the governing mechanical interaction of different biological species involved in atheroma plaque development from both experimental (see Steinberg et al. [6], Zhao

* Correspondence to: Mechanical Engineering department, c/ Maria de Luns s/n. 50015, Zaragoza, Spain.
E-mail addresses: phernand@unizar.es (P. Hernández-López), mcilla@unizar.es (M. Cilla), miguelam@unizar.es (M.A. Martínez), fany@unizar.es (E. Peña), mauro.malve@unavarra.es (M. Malvè).

https://doi.org/10.1016/j.cmpb.2024.108296
Received 31 March 2024; Received in revised form 5 June 2024; Accepted 17 June 2024
Available online 24 June 2024

et al. [7], Howarth et al. [8], among others) and computational perspectives (see [9–12], among others). The complexity of these computational studies varies considerably depending on the number of species considered and the sophistication of the proposed equations [13]. In addition, continuum models, discrete models such as agent-based models, and hybrid models have been proposed. Within the continuum models, Zohdi et al. [14] modeled monocyte adhesion to the endothelial surface controlled by the intensity of blood flow and adhesion molecules stimulated by excess LDL. They also studied monocyte penetration into the intima, subsequent tissue inflammation and plaque rupture, which can lead to thrombus formation or occlusive thrombosis. Their model predicts the time to rupture as a function of arterial geometry, monocyte diameter, adhesion stress, bulk modulus of the ruptured wall material, blood viscosity, flow rate and monocyte mass density. Cobbold et al. [15] and Gessaghi et al. [16] investigated the oxidation process of LDL cholesterol in an in vitro framework, with Cobbold et al. [15] also considering the effect of vitamins E and C. Di Tomaso et al. [10] investigated the interaction between LDL and monocytes, although monocyte behavior was modeled in a very basic way. Fok [17] proposed a mathematical model of intimal thickening as a free boundary problem driven by endothelial damage, cytokine release and SMC migration. More complex studies, such as that of Siogkas et al. [18], included oxidized LDL, macrophages and cytokines, assuming that all LDL molecules and monocytes are oxidized and differentiated as they pass through the endothelium. Calvez et al. [19] presented a similar study from a mathematical point of view, also including foam cells. Ogunrinade et al. [20] used an ordinary differential equation (ODE) model to study cholesterol uptake by different macrophage scavenger receptors in early atherosclerosis and found that macrophage proliferation, rather than increased LDL influx, drives lesion instability. Bulelzai and Dubbeldam [21] developed a qualitative mathematical model comprising several ODEs for the concentrations of key atherosclerotic plaque components: macrophages, monocytes, foam cells and oxidized LDL. Chung and Vafai [12] derived atheroma plaque properties based on microstructural information using a pore theorem and fiber matrix model, taking into account LDL transport. In addition, another study by Chung and Vafai [12] described the effects of Fluid-Structure Interaction (FSI) and pulsation on LDL transport. In terms of agent-based models, Corti et al. [22] developed a CFD model in a 3D arterial model that qualitatively replicated both the physiological and pathological arterial configuration, capturing histological-like features. A variety of agent-based computational models can be found in the literature [23], many of which include a stent [24,25]. Finally, there are some computational models in the literature that consider FSI in atheroma plaques [26,27]. However, most of them only focus on analyzing the stability of plaques as a function of the stresses generated by the blood flow in them, which is the case of Tang et al. [28], Kock et al. [29] and Gao et al. [30]. However, there are also a few models that focus on the influence of hemodynamic changes on atheroma plaque growth. Calvez et al. [19] used a two-dimensional model with mesh displacement due to plaque formation. In addition, [31] analyzed the influence of FSI on LDL flow across the endothelium and its accumulation in the arterial wall and [32] analyzed the influence of FSI on LDL accumulation considering blood flow as a non-Newtonian fluid.

In a previous work [33] a mechanobiological model of atherosclerosis development in the arterial was developed and applied to patient-specific geometries of carotid arteries with the purpose of validation. However, the hemodynamics of blood flow, the inflammatory process of the arterial wall, and the growth of atheroma plaques were computed in an uncoupled and sequential way: the growth of the plaque was calculated only at the end of the inflammatory process. On the contrary, in the development of the real pathology, all these processes are coupled: the growth of a plaque happens at the same time as the inflammatory process and, therefore, it causes changes in hemodynamics which can also affect the evolution of the inflammatory process. In that work, some of the plaques that the real patient had were not accurately predicted by the computational model, and it was hypothesized that this could be because the geometrical and hemodynamic changes produced by the progressive growth of the plaque were not considered. This hypothesis was partially checked by calculating the model again in an uncoupled way and actualizing the geometry and the blood flow at half of the inflammatory process. Therefore, the analyses in the present study have the aim to validate this hypothesis and to determine how changes in the geometry and hemodynamics can affect the growth of plaques. For that, and due to the computational cost of the real models, a simplified model of an axisymmetric carotid artery has been considered instead of a full 3D patient-specific geometry.

2. Materials and methods

The continuum mechanobiological model of atherosclerosis development by Hernández-López et al. [33] has been applied to an axisymmetric model of a carotid artery, using a mechanical stimulus dependent on both, Time Average Wall Shear Stress (TAWSS) and Oscillatory Shear Index (OSI) biomarkers, to determine the areas susceptible of plaque growth. The process of atheroma plaque formation is a complex problem, in which a large quantity of substances and processes are involved. Therefore, only those substances considered to be the most relevant for the process have been included in the model. Among these substances, low-density lipoproteins (LDL) and oxidized low-density lipoproteins (oxLDL), cells like monocytes (m), macrophages (M), foam cells (FC), contractile and synthetic smooth muscle cells (CSMCs and SSMCs, respectively), cytokines (c) and collagen fibers (Cg) are considered. The geometry of the artery and the hemodynamical stimulus are updated as time progresses, to simulate the effects that the atheroma plaque growth causes on blood flow.

Due to the high computational cost that a fully coupled model would require because of the time-scale difference between a cardiac cycle and the inflammatory process in the arterial wall, a semi-coupled model has been developed. The workflow of the computation process is represented in Fig. 1. At the beginning of the process, a total of three cardiac cycles are computed, considering the results of the third cycle to ensure that blood flow is completely developed. Then, with the results of this third cycle, the plasma flow across the endothelium, the inflammatory process of the arterial wall, and the plaque growth are calculated in a coupled way for a determined time lapse, using a moving mesh that allows the geometry to change with the growth of the plaque. Afterward, three new cardiac cycles are computed in the updated geometry and, therefore, the hemodynamics are updated as well. Then, this process is repeated several times until the desired simulation time is reached, imposing in every step as initial concentrations of all substances in the arterial wall the resultant values obtained at the end of the previous step.

2.1. Geometry

Due to the computational requirements that the study would require in the cases of the real geometries [33], a simplified model of an axisymmetric carotid artery has been used. The geometry is primarily used in Hernández-López et al. [34], which corresponds to a carotid artery and it is represented in Fig. 2. It is composed of the arterial lumen and wall, which has been modeled as a mono-layered wall with homogeneous properties, considering the endothelium and the adventitia as membranes. In the considered mechanobiological model, the permeability of the endothelium and, therefore, the development of atheroma plaques, is directly dependent on hemodynamics. Thus, the phenomenon of double stenosis observed in real patients has been included with an obstacle plaque that disturbs blood flow and causes the appearance of a new one downstream [35,36], whose growth is analyzed.

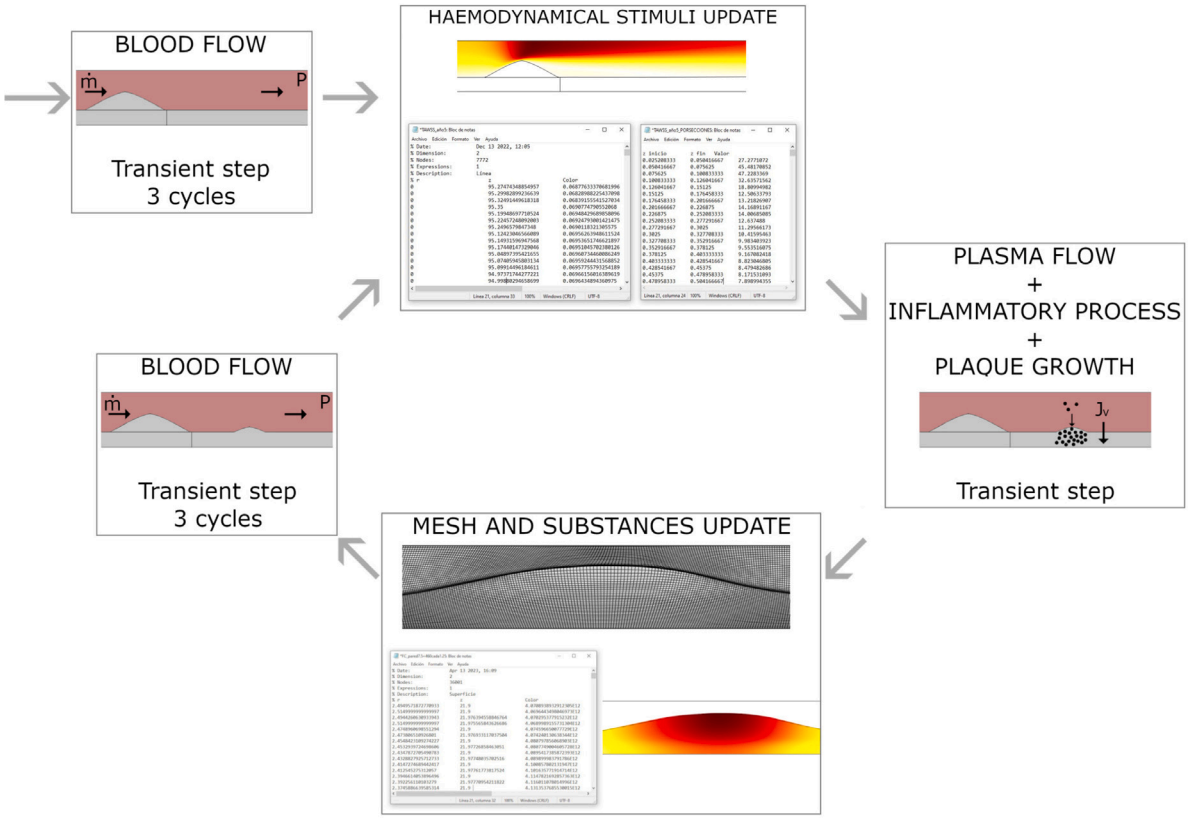

Fig. 1. Workflow of the computational model updating the geometry and the hemodynamics.

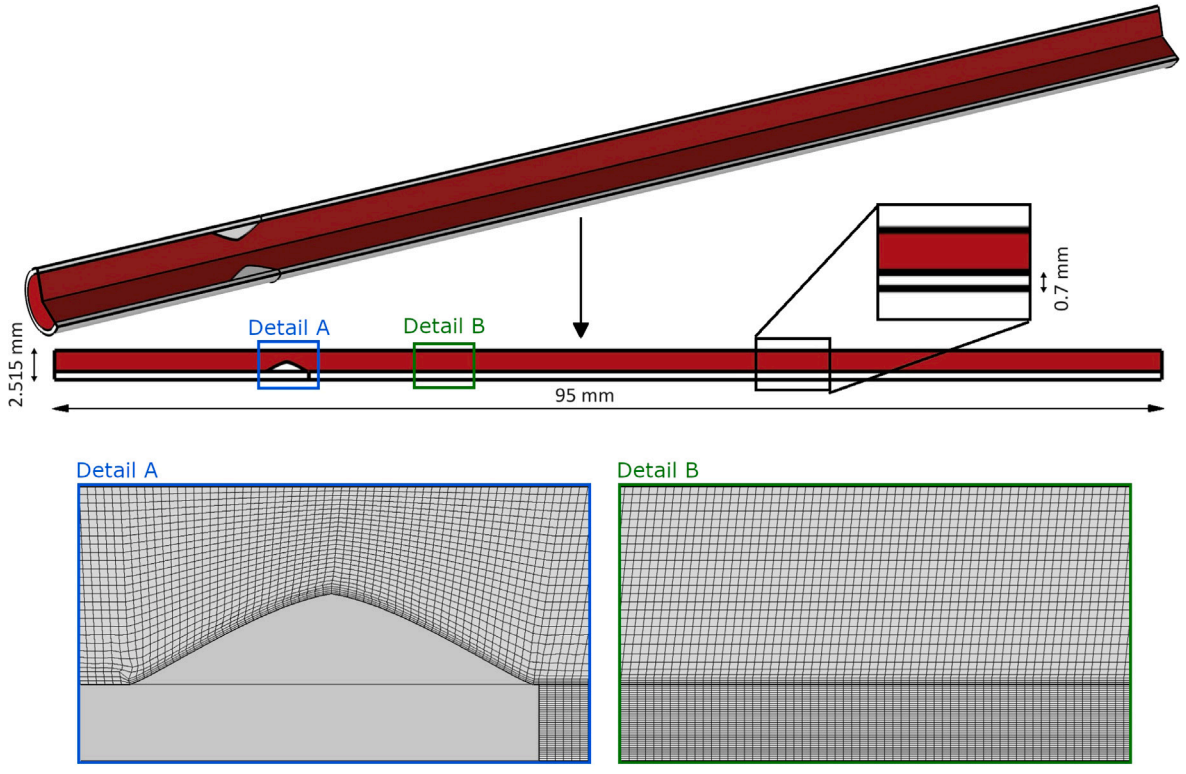

Fig. 2. Two-dimensional axisymmetric geometry. The arterial lumen is represented in red, while the arterial wall and the previous plaque are both represented in white [34].

2.2. Blood flow along the lumen

Due to the behavior of blood in physiological conditions in arteries and to the small size of the particles that conform it compared to the arterial lumen diameter, blood has been considered as a Newtonian, incompressible, and homogeneous fluid [37,38]. Finally, considering the Reynolds number in the case of physiological conditions of blood flow in small arteries (Re ≈ 950 for the mean diameter of the artery considered), blood flow can be considered in the laminar regime [39]. It is ensured that the Reynolds number is consistently maintained below 950 for all geometries and calculations.

Blood flow along the arterial lumen follows Navier–Stokes and continuity equations:

$$\rho_b \frac{\partial \boldsymbol{u_b}}{\partial t} + \rho_b(\boldsymbol{u_b} \cdot \nabla)\boldsymbol{u_b} = \nabla \cdot [-P_b \boldsymbol{I} + \mu_b(\nabla \boldsymbol{u_b} + (\nabla \boldsymbol{u_b})^T)] + \boldsymbol{F_b} \tag{1}$$

$$\rho_b \nabla \cdot \boldsymbol{u_b} = 0, \tag{2}$$

being in all this work the subscripts b and l referred to blood and lumen, respectively. Therefore, ρ_b and μ_b are the density and dynamic viscosity of blood, which take values of 1050 $\frac{\text{kg}}{\text{m}^3}$ and 0.0035 Pa s, respectively [40]. On the other hand, $\boldsymbol{u_b}$ and P_b represent the velocity and pressure of blood flow along the lumen. Finally, $\boldsymbol{F_b}$ is referred to the internal forces of the blood, which can be neglected [41].

Transient velocity and pressure of blood flow in the Internal Carotid Artery (ICA) during a cardiac cycle have been imposed as boundary conditions at the inlet and outlet of the geometry, respectively [39]. In addition, a no-slip boundary condition of blood flow along the endothelium has been imposed.

Fig. 3.a shows the velocity profile at the initial geometry and 3.b shows the Wall Shear Stress (WSS) profile along the artery and the velocity streamlines around the areas with low WSS.

2.3. Plasma flow across the arterial wall

The arterial wall is considered a permeable media taking into account the permeability properties of its constituents [37]. Therefore, certain components of the bloodstream, such as plasma, the liquid component of blood, are able to cross it. Plasma flow across the arterial wall is modeled with Darcy's law and its continuity equation:

$$\boldsymbol{u_p} = -\frac{k_w}{\mu_p} \nabla P_p, \tag{3}$$

$$\frac{\partial(\epsilon_w \rho_p)}{\partial t} + \nabla \cdot (\rho_p \boldsymbol{u_p}) = J_v, \tag{4}$$

being the subscripts w and p referred to the arterial wall and plasma, respectively. Thus, $\boldsymbol{u_p}$ and ∇P_p are the velocity of plasma flow and the pressure gradient in the arterial wall, respectively. On the other hand, k_w represents the Darcy permeability of the arterial wall, μ_p and ρ_p are the dynamic viscosity of plasma and its density, respectively. ϵ_w is the porosity of the arterial wall. Finally, J_v represents the plasma flow through the endothelium and it can be calculated with Kedem–Katchalsky equations for flow through semi-permeable membranes considering the three-pore model [42,43].

The three-pore model considers that the plasma flow can have three different origins depending on the shape of the endothelial cells [44]: In cases of endothelial cells that are normally arranged, e.g. in a healthy artery, plasma flow can go through normal junctions. In other cases in which the endothelial permeability is increased due to a change of the endothelial cells that can be due, among others, to hemodynamic changes, plasma can flow through leaky junctions. Finally, a third flow of plasma may happen across vesicular pathways. However, due to this last way of transport being destined for molecular flow, the quantity of plasma through this way is very small related to the other two, so it is considered negligible:

$$J_v = Jv_{nj} + Jv_{lj} + \cancel{Jv_{vp}}, \tag{5}$$

where Jv_{nj}, Jv_{lj} and Jv_{vp} are the plasma flow through normal junctions, leaky junctions, and vesicular pathways, respectively.

The plasma flow through normal and leaky junctions can be calculated, respectively, as:

$$Jv_{nj} = Lp_{nj} \cdot (\Delta P_{End} - \cancel{\sigma_d \cdot \Delta\Pi}) \cdot (1 - \Phi_{lj}), \tag{6}$$

$$Jv_{lj} = Lp_{lj} \cdot (\Delta P_{End} - \cancel{\sigma_d \cdot \Delta\Pi}), \tag{7}$$

being Lp_{nj} and Lp_{lj} the hydraulic conductivities of normal and leaky junctions, respectively. ΔP_{End} is the pressure drop in the endothelium [45], while term $\sigma_d \cdot \Delta\Pi$ is related to the osmotic pressure, being σ_d the osmotic reflection coefficient of plasma and $\Delta\Pi$ the osmotic pressure differential across the endothelium. However, according to [45], the osmotic term can be considered negligible. Finally, Φ_{lj} is the fraction of leaky junctions in the arterial wall [46–48], which is variable and it has been demonstrated experimentally that it is dependent on different hemodynamical stimuli.

The hemodynamical stimulus considered in this study is the new variable proposed firstly in Hernández-López et al. [33], which is the one that better predicts the plaques in real patients because it combines the effects of TAWSS and OSI. This new variable will be renamed in this work as Combined Hemodynamical Stimulus (CHS). TAWSS and OSI are calculated by knowing the tangential stress vector of blood flow in the endothelium ($\tau(t)$) and the period of a cardiac cycle (T) as:

$$TAWSS = \frac{1}{T} \int_o^T |\tau(t)| \cdot dt, \tag{8}$$

$$OSI = 0.5 \cdot \left(1 - \frac{|\frac{1}{T} \int_o^T \tau(t) \cdot dt|}{TAWSS}\right) \tag{9}$$

The ratio Φ_{lj} and CHS are related by a pseudo-experimental correlation defined in Hernández-López et al. [33], depending on the shape index of the endothelial cells (SI), which can be defined as:

$$SI = \frac{4\pi \cdot Area}{Perimeter^2}, \tag{10}$$

where $Area$ and $Perimeter$ are those referred to a singular cell, being SI equal to 1 in the case of a circular cell and 0 for a linear cell.

The shape of the endothelial cells can be determined depending on CHS with a pseudo-experimental correlation, being low values of TAWSS and high values of OSI considered as atheroprones [49–51]:

$$SI(CHS) = 0.0264 \cdot e^{5.647 \cdot OSI} + 0.5513 \cdot e^{-0.1815 \cdot TAWSS^2}, \tag{11}$$

In addition, an experimental correlation determines the number of endothelial mitotic cells (MC) in areas of known SI [52]:

$$MC = 0.003797 \cdot e^{(14.75 \cdot SI)} \tag{12}$$

The relation between the number of mitotic cells and leaky cells in the endothelium can be determined with the next experimental correlation [44,53]:

$$LC = 0.307 + \frac{0.805 \cdot MC}{0.453} \tag{13}$$

On the other hand, Φ_{lj} can be calculated as [46–48]:

$$\Phi_{lj} = \frac{LC \cdot \pi \cdot R_{cell}^2}{A_{unit}}, \tag{14}$$

where R_{cell} is the radius of an endothelial cell and A_{unit} represents a unit area considered in the experimental correlations (0.64 mm^2). Therefore, the plasma flow through normal junctions is completely determined. On the other hand, to determine the plasma flow through leaky junctions, it is still necessary to determine Lp_{lj}, which can be calculated as:

$$Lp_{lj} = \frac{Ap}{S} \cdot Lp_{slj}, \tag{15}$$

where $\frac{Ap}{S}$ is the ratio between the total area comprising the leaky junction compared to the total area available for it, while Lp_{slj} is the

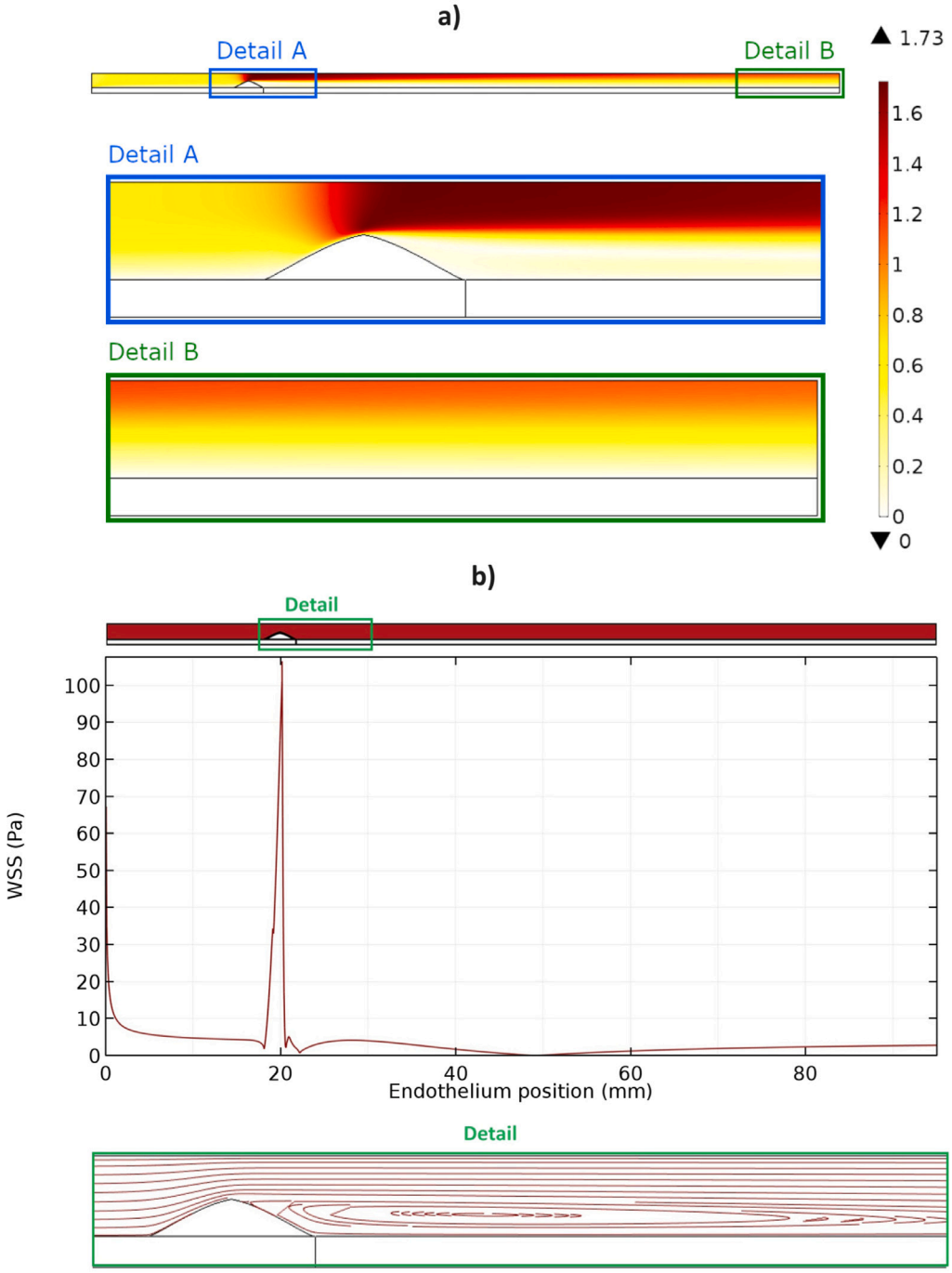

Fig. 3. (a) Velocity profile along the artery. (b) WSS distribution and velocity streamlines.

hydraulic conductivity that corresponds to a singular leaky junction. The values of both parameters can be determined by assuming that leaky junctions surround the leaky cells and, therefore, they have a ring shape [46,54]. Thus, the fraction of area comprising the leaky junction and the total area available for it can be computed as:

$$\frac{A_p}{S} = \frac{A_{slj}}{\pi \cdot {\varepsilon_{lj}}^2}, \tag{16}$$

being ε_{lj} the half distance between two leaky junctions that are aleatory distributed and A_{slj} the area of a singular leaky junction, which can be calculated, knowing the half-width of a leaky junction (w_l) as:

$$A_{slj} = \pi \cdot (R_{cell} + 2 \cdot w_l)^2 - \pi \cdot R_{cell}^2 = 2\pi \cdot R_{cell} \cdot 2w_l + w_l^2 \approx 2\pi \cdot R_{cell} \cdot 2w_l \tag{17}$$

Thus, Eq. (16) can be rewritten as:

$$\frac{A_p}{S} = \frac{4 \cdot R_{cell} \cdot w_l}{{\varepsilon_{lj}}^2} \tag{18}$$

However, ε_{lj}^2 is not known. Φ_{lj} can be calculated too as the ratio between the area of a leaky cell and the area available for it [46,47]:

$$\Phi_{lj} = \frac{{R_{cell}}^2}{{\varepsilon_{lj}}^2} \Rightarrow {\varepsilon_{lj}}^2 = \frac{{R_{cell}}^2}{\Phi_{lj}} \tag{19}$$

Therefore:

$$\frac{A_p}{S} = \frac{4w_l}{R_{cell}} \cdot \Phi_{lj}, \tag{20}$$

Table 1
List of the parameters necessary to calculate plasma flow through the endothelium.

Parameter	Description	Value	Reference
Physic properties			
k_w	Darcy permeability	$1.2 \cdot 10^{-18}$ m^2	[47] [55]
$L_{p,nj}$	Normal junction conductivity	$1.984 \cdot 10^{-12}$ $\frac{m}{s\,Pa}$ [a,b]	[45]
ϵ_w	Intima porosity	0.96	[56]
μ_p	Plasma dynamic viscosity	0.001 Pa s	[40]
ρ_p	Plasma density	1050 $\frac{kg}{m^3}$	[40]
Dimensions			
A_{unit}	Unit area for the experimental correlations	0.64 mm^2	[44,53]
l_{lj}	Length of a leaky junction	2 μm	[46]
R_{cell}	Endothelial cell radius	15 μm	[46]
w_l	Half-width of a leaky junction	20 nm	[46]
Pressures			
P_{adv}	Pressure of the adventitia	17.5 mmHg	[44]
ΔP_{End}	Pressure drop in the endothelium	20.727 mmHg[b]	[45]

[a] The value of the parameter is dependent on the considered artery (carotid arteries).
[b] The value of the parameter is dependent on the intraluminal pressure (100 mmHg).

and Eq. (15) can be written as:

$$Lp_{lj} = \frac{4w_l}{R_{cell}} \cdot \Phi_{lj} \cdot Lp_{slj} \tag{21}$$

Finally, the hydraulic conductivity of a singular leaky junction, Lp_{slj}, can be calculated as [44]:

$$Lp_{slj} = \frac{w_l^2}{3 \cdot \mu_p \cdot l_{lj}}, \tag{22}$$

where l_{lj} is the length of a leaky junction in the perpendicular direction to the endothelium.

The pressure at the adventitia is set as a boundary condition [44]. All the parameters involved in the determination of plasma flow across the endothelium are included in Table 1.

2.4. Molecular flows across the endothelium

Due to the increase in the endothelial permeability of the atheroprones areas of the arterial wall, some substances that are normally contained in the bloodstream can pass from the lumen into the arterial wall, across the endothelium. It is the case of LDL and monocytes.

The flow of LDL molecules across the endothelium can be modeled with the three-pore model, in the same way as for plasma flow [44]. In this case, due to the size of LDL molecules, its transport can only take place through leaky junctions and vesicular pathways [20,57]:

$$Js = \cancel{Js_{nj}} + Js_{lj} + Js_{vp}, \tag{23}$$

being Js_{nj}, Js_{lj} and Js_{vp} the flows of LDL across the normal junctions, leaky junctions and vesicular pathways, respectively. These flows can be calculated with the Kedem–Katchalsky Equation [43]:

$$Js,i = C_{LDLdep} \cdot P_{app,i} \tag{24}$$

where C_{LDLdep} is the concentration of LDL molecules deposited in the arterial wall and it is dependent of the LDL concentration in the lumen which, in this work, has been taken equal to 6.98 $\frac{mol_{LDL}}{m^3}$ [58]. $P_{app,i}$ is the coefficient of apparent permeability of the arterial wall across leaky junctions and vesicular pathways ($P_{app,lj}$ and $P_{app,vp}$, respectively). In addition, it is known that the flow of LDL through vesicular pathways corresponds to the 10% of LDL flow through leaky junctions [59]:

$$P_{app,vp} = 0.1 \cdot P_{app,lj} \tag{25}$$

It is possible to determine the apparent permeability of leaky junctions, depending on its diffusive permeability (P_{lj}), a reduction factor of LDL concentration gradient at the entrance of LDL flow (Z_{lj}), and the solvent-drag coefficient of leaky junctions ($\sigma_{f,lj}$) [57,60]:

$$P_{app,lj} = P_{lj} Z_{lj} + J_{v,lj} \cdot (1 - \sigma_{f,lj}) \tag{26}$$

Therefore, the flow of LDL molecules across the endothelium can be rewritten as:

$$J_{S,LDL} = 1.1 \cdot C_{LDLdep} \cdot (P_{lj} Z_{lj} + J_{v,lj}(1 - \sigma_{f,lj})) \tag{27}$$

The diffusive permeability of leaky junctions can be calculated as [44]:

$$P_{lj} = \frac{A_p}{S} \chi P_{slj}, \tag{28}$$

being χ the difference between the total area of endothelial cells and the area of endothelial cells separated by leaky junctions, and P_{slj} the permeability of a leaky junction. The parameter χ can be calculated as:

$$\chi = 1 - \alpha_{lj}, \tag{29}$$

where α_{lj} represents the proportion of pore area occupied by LDL molecules, and can be determined by knowing the radius of an LDL molecule and the half-width of a leaky junction, already defined [44]:

$$\alpha_{lj} = \frac{R_{LDL}}{w_l} \tag{30}$$

On the other hand, the permeability of a leaky junction can be calculated by knowing its length (l_{lj}), and the diffusion coefficient of LDL in it, P_{slj}:

$$P_{slj} = \frac{D_{lj}}{l_{lj}} \tag{31}$$

It is possible to determine the diffusion coefficient of LDL in a leaky junction with the next empirical correlation, that relates it to the LDL diffusion coefficient in the whole arterial wall (D_l) [61]:

$$\frac{D_{lj}}{D_l} = F\left(\alpha_{lj}\right) = 1 - 1.004\alpha_{lj} + 0.418\alpha_{lj}^3 - 0.16\alpha_{lj}^5 \tag{32}$$

On the other hand, the reduction factor of the LDL concentration gradient Z_{lj}, required due to the endothelium's nature as a biological membrane with pores, can be calculated as follows [57]:

$$Z_{lj} = \frac{Pe_{lj}}{e^{(Pe_{lj})} - 1} \tag{33}$$

As can be seen, this reduction factor depends on a modified Peclet number, which is defined as [57]:

$$Pe_{lj} = \frac{Jv,lj \cdot (1 - \sigma_{f,lj})}{P_{lj}} \tag{34}$$

Finally, the solvent-drag reflection coefficient of leaky junctions determines the natural selectivity of the endothelium to the flow of substances across it, being molecules with a reflection coefficient higher than one excluded by the endothelium. It can be calculated with the next equation [44]:

$$\sigma_{f,lj} = 1 - \frac{2}{3}\alpha_{lj}^2(1 - \alpha_{lj}) \cdot F(\alpha_{lj}) - (1 - \alpha_{lj})\left(\frac{2}{3} + \frac{2\alpha_{lj}}{3} - \frac{7\alpha_{lj}^2}{12}\right), \tag{35}$$

where all the variables have already been defined.

After LDL enters the arterial wall, it transforms into oxLDL. Then, due to the presence of oxLDL in the arterial wall, there is a flow of monocytes (which are naturally in the bloodstream) from the lumen into the arterial wall, across the endothelium. This monocyte flow depends also on the hemodynamics, because it is higher in areas of higher LDL flow across the endothelium and, considering CHS as the main hemodynamical stimulus, it can be modeled with the next

Table 2
Summary of the equations of the inflammatory process in the arterial wall.

Substance	Time	Diffusion	Convection	Source–sink
LDL	$\frac{\partial C_{LDL,w}}{\partial t}$	$\nabla \cdot (-D_{LDL,w} \nabla C_{LDL,w})$	$k_{lag,LDL} \cdot \boldsymbol{u_p} \cdot \nabla C_{LDL,w}$	$-d_{LDL} C_{LDL,w}$
Oxidized LDL	$\frac{\partial C_{oxLDL,w}}{\partial t}$	$\nabla \cdot (-D_{oxLDL,w} \nabla C_{oxLDL,w})$	–	$d_{LDL} C_{LDL,w} k_{(LDL-oxLDL)}$ $-LDL_{ox,r} C_{oxLDL_w} C_{M,w}$
Monocytes	$\frac{\partial C_{m,w}}{\partial t}$	$\nabla \cdot (-D_{m,w} \nabla C_{m,w})$	–	$-d_m C_{m,w}$ $-m_d C_{m,w}$
Macrophages	$\frac{\partial C_{M,w}}{\partial t}$	$\nabla \cdot (-D_{M,w} \nabla C_{M,w})$	–	$d_m C_{m,w} k_{(m-M)}$ $-\frac{LDL_{ox,r}}{n_{FC}} \cdot C_{oxLDL_w} C_{M,w}$
Cytokines	$\frac{\partial C_{c,w}}{\partial t}$	–	–	$C_r C_{oxLDL_w} C_{M,w}$ $-d_c C_{c,w}$
CSMCs	$\frac{\partial C_{CSMC,w}}{\partial t}$	–	–	$-C_{CSMC,w} \cdot S_r \cdot \left(\frac{C_{c,w}}{k_c \cdot C_{c,w}^{th} + C_{c,w}} \right)$
SSMCs	$\frac{\partial C_{SSMC,w}}{\partial t}$	–	–	$C_{CSMC,w} \cdot S_r \cdot \left(\frac{C_{c,w}}{k_c \cdot C_{c,w}^{th} + C_{c,w}} \right) \cdot k_{(SMC)}$ $+ \left(\frac{p_{ss} C_{c,w}}{C_{c,w/2}^{th} + C_{c,w}} \right) C_{SSMC,w} \left(1 - \frac{C_{SSMC,w}}{C_{SSMC,w}^{th}} \right)$ $-r_{Apop} \cdot C_{SSMC,w}$
FCs	$\frac{\partial C_{FC,w}}{\partial t}$	–	–	$\frac{LDL_{ox,r}}{n_{FC}} \cdot C_{oxLDL_w} C_{M,w} \cdot k_{(M-FC)}$
Collagen	$\frac{\partial C_{Cg,w}}{\partial t}$	–	–	$G_r \cdot C_{SSMC,w}$ $-d_{Cg} \cdot C_{Cg,w}$

equation [33]:

$$J_{s,m}(TAWSS, OSI) = m_r \cdot (0.8588 \cdot e^{-0.6301 \cdot TAWSS} + 0.1295 \cdot e^{3.963 \cdot OSI}) \cdot C_{LDL,ox,w} \cdot C_{m,l}, \quad (36)$$

being m_r the monocyte recruitment from the lumen, $C_{LDL,ox,w}$ the concentration of oxLDL in the arterial wall and $C_{m,l}$ the monocyte concentration in the lumen which, in this work, has been considered as $550 \cdot 10^9 \ \frac{Monocyte}{m^3}$ [62].

2.5. Inflammatory process of the arterial wall

Once the LDL and monocytes are present in the arterial wall, the inflammatory process in the arterial wall starts. As commented in the Introduction section, there are many substances and cells involved in this process, whose behavior can be modeled with convection–diffusion–reaction equations:

$$\underbrace{\frac{\partial C_i}{\partial t}}_{Time} + \underbrace{\nabla \cdot (-D_i \nabla C_i)}_{Diffusion} + \underbrace{k_{lag,i} \cdot \boldsymbol{u_p} \cdot \nabla C_i}_{Convection} = \underbrace{f_{Ci}(\cdots, C_i, \ldots)}_{Source--sink}, \quad (37)$$

where C_i and D_i represent, respectively, the concentration and the diffusion coefficient in the arterial wall of the considered substance. The first term of the equation considers temporal variations of the substances in the arterial wall. Its second term corresponds to the diffusion of the considered substance in the arterial wall. Due to the arterial wall layers and cell arrangement, the longitudinal diffusion of substances in it is favored over the radial one, so diffusion of substances in the arterial wall has been considered anisotropic. According to [54], the ratio between the longitudinal and radial diffusion coefficients in the media layer of the arterial wall is approximately equal to 3. The third term of Eq. (37) represents substance convection in the arterial wall. The convection of a substance in a free medium is not the same as in a porous one like the arterial wall. Thus, $k_{lag,i}$ limits the convection in the arterial wall related to the convection in a free medium, and it is named the solute lag coefficient of the considered substance in the arterial wall [44,63,64]. Finally, the last term of Eq. (37) is a reactive term that represents the different interactions that the substances can suffer in the arterial wall, which encompasses different phenomena depending on the considered substance. The specific equations for all the substances considered in the model are included in Table 2.

As can be observed in Table 2, the only substance considered to suffer convection is LDL, due to its small size. In addition, LDL, oxidized LDL, monocytes, and macrophages experience diffusion in the arterial wall [58]. LDL that gets oxidized when enters the arterial wall is represented in the reactive term of LDL and, also, in the first reactive term of oxLDL equation. On the other hand, the quantity of oxidized LDL that is phagocyted by macrophages is represented by the second reactive term of oxLDL. The differentiation of monocytes into macrophages corresponds to the first reactive term of both, monocyte and macrophage equations, while monocyte apoptosis is represented with their second reactive term. To end with the macrophages, the quantity of them that become foam cells after phagocyte as maximum oxidized LDL as possible is represented in the second term of macrophages reactive terms, which is, also, the reactive term of foam cells. On the other hand, the cytokines that are segregated in the arterial wall due to the presence of oxidized LDL in it are represented by their first reactive term, while their natural degradation is represented in the second reactive term of their equation. The change of smooth muscle cells (SMC) from contractile to synthetic is represented in the first reactive term of both, CSMC and SSMC, while SSMC also have proliferation and apoptosis (represented in their second and third terms, respectively). In addition, collagen fibers are segregated by SSMC and have natural degradation (first and second collagen reactive terms, respectively).

There are some conversion parameters in the equations of the inflammatory process in the arterial wall to achieve their unit consistency, whose value is therefore equal to 1. It is the case of $k_{(LDL-oxLDL)}$, which represents that when a molecule of LDL gets oxidized, it turns into another one molecule of oxidized LDL. $k_{(m-M)}$ represents the differentiation of a monocyte into a macrophage, $k_{(SMC)}$ is the conversion parameter for the change of phenotype of a contractile smooth muscle cell into a synthetic one, and $k_{(M-FC)}$ determine that the death of a macrophage due to the oxidized LDL ingested turns into a foam cell.

To finally define the inflammatory process in the arterial wall, it is necessary to define some boundary conditions: There is no substance flow across the adventitia because it has been considered an impermeable membrane [58]. The convection velocity of LDL in the arterial wall corresponds to that of plasma flow, already determined. LDL concentration in the adventitia, $C_{LDL,adv}$, has been imposed, following the experimental LDL distribution across the arterial wall of Meyer et al. [65]. At the beginning of the inflammatory process, the artery is considered a healthy artery. Therefore, CSMCs are the only substance

Table 3
List of the parameters that are needed to calculate the inflammatory process in the arterial wall.

Parameter	Description	Value	Reference
Substances properties and dimensions			
$D_{r,LDL,w}$ $D_{r,oxLDL,w}$	LDL and oxLDL diffusion coefficients in the radial direction of the arterial wall	$8 \cdot 10^{-13}$ $\frac{m^2}{s}$	[55]
$D_{\theta,LDL,w}$ $D_{\theta,oxLDL,w}$	LDL and oxLDL diffusion coefficients in the circumferential direction of the arterial wall	$2.4 \cdot 10^{-12}$ $\frac{m^2}{s}$	[55] [54]
$D_{z,LDL,w}$ $D_{z,oxLDL,w}$	LDL and oxLDL diffusion coefficients in the longitudinal direction of the arterial wall	$2.4 \cdot 10^{-12}$ $\frac{m^2}{s}$	[55] [54]
$D_{r,m,w}$ $D_{r,M,w}$	Monocyte and macrophage diffusion coefficients in the radial direction of the arterial wall	$8 \cdot 10^{-15}$ $\frac{m^2}{s}$	[58]
$D_{\theta,m,w}$ $D_{\theta,M,w}$	Monocyte and macrophage diffusion coefficients in the circumferential direction of the arterial wall	$2.4 \cdot 10^{-14}$ $\frac{m^2}{s}$	[58] [54]
$D_{z,m,w}$ $D_{z,M,w}$	Monocyte and macrophage diffusion coefficients in the longitudinal direction of the arterial wall	$2.4 \cdot 10^{-14}$ $\frac{m^2}{s}$	[58] [54]
$k_{lag,LDL}$	Solute lag coefficient of LDL	0.893	[64]
l_{lj}	Length of a leaky junction	2 μm	[46]
Mw_{LDL}	LDL molecular weight	386.65 $\frac{g}{mol_{LDL}}$	[41]
R_{LDL}	LDL radius	11 nm	[57]
w_l	Half-width of a leaky junction	20 nm	[46]
ρ_{LDL}	LDL density	1063 $\frac{kg}{m^3}$	[66]
Initial and threshold concentrations			
$C_{0,CSMC}$	CSMC initial concentration	$3.16 \cdot 10^{13}$ $\frac{CSMC}{m^3}$	[67]
$C_{c,w}^{th}$	Cytokine threshold	$1.235 \cdot 10^{13}$ $\frac{mol_C}{m^3}$ *	[33]
$C_{LDL,adv}$	LDL concentration at adventitia	11.6 ,**·C_{LDLdep}	[65]
$C_{SSMC,w}^{th}$	SSMC threshold	$4.764 \cdot 10^{13}$ $\frac{SSMC}{m^3}$	[68]
$C_{0,LDL}$	LDL pathological concentration in blood	6.98 $\frac{mol}{m^3}$	[41]
$C_{0,m}$	Monocyte concentration in blood	$550 \cdot 10^9$ $\frac{cells}{m^3}$	[62]
Lumen-Arterial wall flow			
C_{LDLdep}	LDL deposited at the endothelium	$10^{-2} \cdot C_{LDL,l}$	[65]
m_r	Monocyte recruitment	$6.636 \cdot 10^{-4}$ $\frac{m^4}{mol_{oxLDL} \cdot d}$ *	[6]
Parameters of reactive terms			
C_r	Cytokine production	$3 \cdot 10^{-10}$ $\frac{mol_C \cdot m^3}{mol_{oxLDL} \cdot Macrophage \cdot s}$	[58]
d_c	Cytokine degradation	$2.3148 \cdot 10^{-5}$ s^{-1}	[69]
d_{Cg}	Collagen degradation	$\frac{1}{30}$ d^{-1}	[1]
d_{LDL}	LDL oxidation frequency	$2.85 \cdot 10^{-4}$ s^{-1}	[56]
d_m	Monocyte differentiation frequency	$1.15 \cdot 10^{-6}$ s^{-1}	[21]
G_r	Collagen production	$2.472 \cdot 10^{-21}$ $\frac{kg_{Cg}}{SSMC \cdot s}$	[70]
k_c	Citokyne threshold factor	0.65093	[33]
$LDL_{ox,r}$	Oxidized LDL uptake	$2.45 \cdot 10^{-23}$ $\frac{m^3}{Macrophage \cdot s}$	[7]
m_d	Monocyte natural death frequency	$\frac{1}{60}$ d^{-1}	[71]
n_{FC}	Maximum oxidized LDL uptake	$2.72 \cdot 10^{-11}$ $\frac{mol_{oxLDL}}{Macrophage}$	[72]
p_{ss}	SSMC proliferation	0.24 d^{-1}	[73]
r_{apop}	SSMC apoptosis rate	$0.087d^{-1}$	[74]
S_r	SMC differentiation	0.0036 d^{-1}	[58]

* The values of these parameters are dependent on the considered artery (carotid arteries).
** The value of the parameter is dependent on the intraluminal pressure (100 mmHg).

of the model that has an initial concentration in the arterial wall. There is only LDL and monocytes transport across the endothelium due to the rest of the substances are not present in the bloodstream. All the parameters that are needed to determine and calculate all the inflammatory processes in the arterial wall are included in Table 3.

It should be noted that the influence of the parameters of this mathematical model was studied in a previous work of the same authors [34].

Finally, for the sake of clarity, Fig. 4 shows a summary of the applied boundary conditions.

2.6. Arterial wall mechanical model

In this study, due to the simplification of considering axisymmetric geometry, the arterial wall has been modeled considering Yeoh's model for compressible, isotropic, and hyperelastic materials, whose strain energy density function is [75]:

$$\Psi = \sum_{i=1}^{3} C_{Yeoh,i} \cdot \left[I_1 - 3\right]^i + \frac{1}{2} \cdot K_w (1 - J)^2, \tag{38}$$

where I_1 is the first invariant of the right Cauchy–Green deformation tensor. $C_{Yeoh,i}$ are three material constants that were determined from experimental data, and take values of 17.005 kPa, −73.424 kPa and 414.952 kPa [67]. In addition, it is necessary to define the value of the initial compression modulus of the arterial wall, K_w. There are some studies in the literature, like [76] that show that the arterial wall is compressible and that it suffers a mean volumetric variation, J, of 9.31%. K_w was fitted in order to find the value of initial compression of the arterial wall that corresponds to the experimental volumetric variation, obtaining a value of 44.6 kPa.

To compute the arterial wall mechanics in the model it is also necessary to fix both ends of the model in the longitudinal axis of the artery (to avoid the rigid body movement).

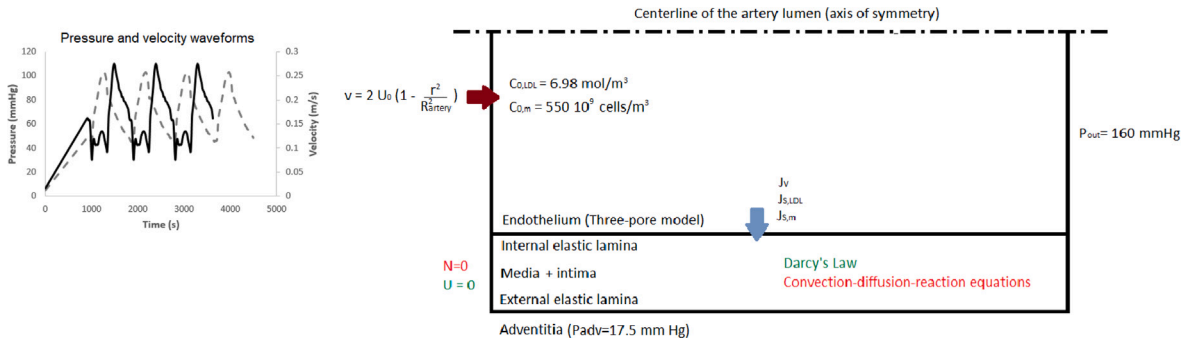

Fig. 4. Summary of the applied boundary conditions.

Table 4
List of the parameters that are needed to calculate plaque growth in the arterial wall.

Parameter	Description	Value	Reference
l_{SSMC}	SSMC length	115 μm	[58]
R_{FC}	Foam cell radius	15.264 μm	[79]
			[72]
R_{SSMC}	SSMC radius	3.75 μm	[58]
ρ_{Cg}	Collagen density	1000 $\frac{kg}{m^3}$	[80]

2.7. Plaque initiation and growth

Finally, once the concentrations of all substances in the arterial wall are known, it becomes possible to determine the growth of atheroma plaques within it. Although all the substances and cells that are present in the inflammatory process of the arterial wall contribute to add volume to the plaque, in this study only the greatest are considered: FC, SSMC, and collagen fibers. Considering isotropic growth of the arterial wall due to plaques formation, the volumetric growth of atheroma plaques (v) can be defined as:

$$\nabla \cdot v = \frac{\partial C_{FC,w}}{\partial t} \cdot v_{FC} + \frac{\partial C_{SSMC,w}}{\partial t} \cdot v_{SSMC} + \frac{\partial C_{Cg,w}}{\partial t} \cdot \frac{1}{\rho_{Cg}}, \tag{39}$$

where $C_{i,w}$ is the concentration of the considered substance in the arterial wall. v_{FC}, v_{SSMC}, and ρ_{Cg} are, respectively, the volumes of a single FC and SSMC and the collagen density. To determine the volumes of an FC and an SSMC, they are assumed to have spherical [77] and ellipsoid [78] shapes, respectively:

$$v_{FC} = \frac{4}{3}\pi {R_{FC}}^3 \tag{40}$$

$$v_{SSMC} = \frac{4}{3}\pi {R_{SSMC}}^2 \cdot l_{SSMC}, \tag{41}$$

where R_{FC} and R_{SSMC} are the radius of an FC and an SSMC, respectively, while l_{SSMC} is the length of an SSMC. All the parameters that are needed to calculate the growth of atheroma plaques in arteries are included in Table 4.

2.8. Endothelial repair after hemodynamic changes

Accordingly with the previous sections, due to changes in hemodynamics caused by the progressive growth of an atheroma plaque, the SI of the endothelial cells may change over time. Some areas considered as atheroprones at the beginning of the process (due to having an elevated SI), can turn into areas considered as atheroprotectives later (with a low SI value). Thus, in these areas, the permeability of the endothelium may be lower at the end than at the beginning of the process and, therefore, it can be considered as an endothelial repair produced by changes in the hemodynamics.

There are some studies that mention endothelial repair due to hemodynamic changes [17]. However, there is no clear evidence about endothelial repair due to changes in hemodynamics or the way in which it occurs and how can this affect endothelial permeability. Himburg et al. [81] show that the endothelium has an adaptation period in which its permeability changes over time due to a change in the values of WSS. Cunningham and Gotlieb [82] stated that areas with low values of WSS are atheroprones due to that they affect, among others, the endothelial cell repair. They also mention that, according to Langille et al. [83], these endothelial changes are reversible when hemodynamics change. VanEpps and Vorp [84] mention that the change in endothelial permeability due to changes in hemodynamics is potentially due to the contacts between endothelial cells, and that shear stress can change the proliferation and apoptosis of endothelial cells. In addition, Slager et al. [85] mention that, according to Bürrig [86], Tricot et al. [87], there are changes in the endothelial cells on the top of a plaque when the plaque enters into the lumen, which can change the endothelial properties of that area and protect endothelial cells against apoptosis.

The geometry and hemodynamic variables of the model have been updated several times. This is done by calculating the FSI, taking into account the growth of the atheroma plaque up to the time of the update. Then the areas of low TAWSS and OSI change. In addition, to determine how the update frequency of the geometry and the hemodynamics affect the growth of the plaque, the stenosis ratio of the generated plaque, which represents the area of the lumen occluded by the plaque, is analyzed in all cases and is defined as:

$$SR(\%) = \left(1 - \frac{Area\,of\,lumen\,with\,plaque}{Area\,of\,healthy\,lumen}\right) \cdot 100 \tag{42}$$

Due to this, as the endothelium behavior due to hemodynamical changes is not completely known, the two extreme cases of endothelial repair have been considered in this work:

- Endothelial repair model: In this model, once the hemodynamic stimuli that cause plaque growth are removed, endothelial permeability in the area immediately decreases, suggesting that the endothelium repairs itself. In essence, the endothelium quickly returns to a normal, less permeable state once the damaging stimuli are removed. This model takes into account only the current values of the hemodynamic stimuli, derived from the most recent geometry update.
- Model without endothelial repair: In contrast, this model assumes that endothelial permeability remains high even after the hemodynamic stimuli that induce plaque growth have ceased, due to permanent endothelial damage. Thus, it does not take into account endothelial repair. For this model, it is necessary to track historical values of TAWSS and OSI with each geometry update. This involves keeping a record of the highest endothelial permeability associated with each section of the geometry. As areas of low TAWSS and high OSI are prone to atherosclerosis, the minimum historical values of TAWSS and the maximum historical values of OSI are used in this model.

In addition to the models with and without endothelial repair, a third scenario was considered. Specifically, we refer to the uncoupled model, which does not update the areas of low WSS due to atheroma plaque growth and does not include FSI.

2.9. Numerical methods

The software COMSOL Multiphysics (COMSOL AB, Burlington, MA, USA) has been used to computationally solve the model. The Multifrontal Massively Parallel Sparse Direct Solver (MUMPS, MUM [88]) was used for both time steps, using the implicit backward differentiation formula method (BDF, Curtiss and Hirschfelder [89]) to solve them, with Newton's method for non-linear problems. In addition, the inflammatory process of the arterial wall, the plaque growth and the moving mesh are calculated by dividing them into different groups of separated steps. The total simulation time was 10 years and the time step size was 10 days.

Due to the semi-coupled process, different time intervals of geometry and hemodynamics updates can lead to different results: Shorter update intervals will provide results more similar to the ones obtained with a fully coupled model. But shorter update intervals will also require more computational cost. Thus, to analyze how the update frequency intervals affect the results, the model has been solved with update periods of 10, 5, 2.5, and 1.25 years. It should be noted that each time the model is updated, a new FSI calculation is performed. This recalculation takes into account changes in the regions of low WSS due to the growth of the atheroma plaque, which in turn affects the areas where the plaque will continue to grow.

The geometry has been discretized using the finite element method, with quadrilateral elements to mesh the lumen and the arterial wall. A sensitivity analysis of both, lumen and arterial wall meshes, has been performed, employing the criterion of ensuring less than a 5% variation in results between two consecutive meshes. In addition, to correctly determine the hemodynamics near the endothelium that leads to a change in its permeability some boundary layers have been included in the lumen mesh, in the area near the endothelium. After the sensitivity analysis, the selected meshes are composed of 35,435 elements and 36,001 elements, for the lumen and the arterial wall, respectively, and a total of three boundary layers are used near the endothelium (see Fig. 2).

The smoothing method selected to compute the deformation of the moving mesh is Laplace smoothing, which requires a small computational cost because the displacement of each mesh node in one direction is not coupled with the one in the other direction. Therefore, the next equations are solved in all the nodes of the mesh:

$$\frac{\partial^2}{\partial X^2}\frac{\partial x}{\partial t} + \frac{\partial^2}{\partial Y^2}\frac{\partial x}{\partial t} = 0 \tag{43}$$

$$\frac{\partial^2}{\partial X^2}\frac{\partial y}{\partial t} + \frac{\partial^2}{\partial Y^2}\frac{\partial y}{\partial t} = 0 \tag{44}$$

being x and y the coordinates of the nodes in the deformed mesh, and X and Y the coordinates of the nodes in the reference mesh.

3. Results

Fig. 5 shows the wall thickness increase in the area of plaque growth for the uncoupled model with a total simulation time of 10 years. As visible, the maximum wall thickness increase is 0.70 mm, which corresponds to a stenosis ratio of 62.58%.

Figs. 6 and 7 show the results of the stenosis ratio obtained for a total simulation time of 10 years with all the intermediate results depending on the update geometry period (every 5, 2.5, and 1.25 years), considering endothelial repair (Fig. 6) and not considering it (Fig. 7). In addition, the stenosis ratio obtained for 10 years in the uncoupled model is also shown. In Fig. 6 it can be seen that the stenosis ratio is higher in the uncoupled model than in the FSI model with endothelial repair. Furthermore, for the case of the FSI with endothelial repair, the stenosis ratio decreases as the time between geometry updates decreases, with convergence being reached in the case of geometry updates every 2.5 years. On the contrary, as it can be seen in Fig. 7, the stenosis ratio obtained for the case of FSI without endothelial repair is larger than those obtained in the uncoupled model. Moreover, it can be seen that the stenosis ratio of the plaque increases if the frequency of geometry updating increases, and, in the case of updating the geometry every 1.25 years, the stenosis ratio for the year 10 is almost 100%.

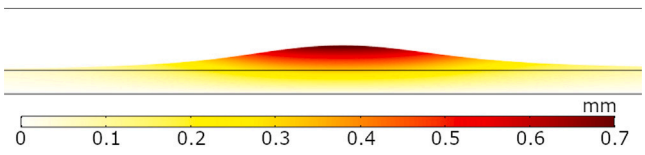

Fig. 5. Arterial wall thickness increase for the uncoupled model for a time of simulation of 10 years.

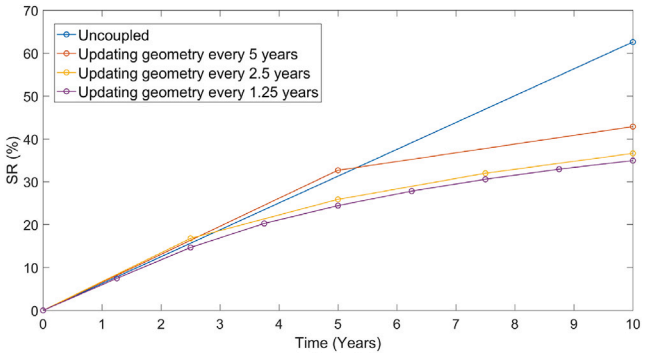

Fig. 6. Stenosis ratio obtained for the uncoupled and FSI with endothelial repair models, for all the temporal intervals of geometry updating.

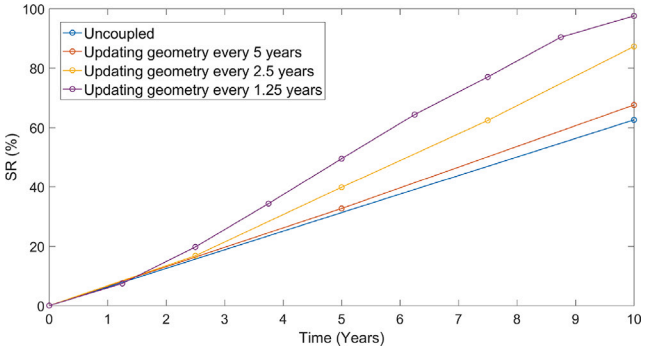

Fig. 7. Stenosis ratio obtained for the uncoupled and FSI without endothelial repair models, for all the temporal intervals of geometry updating.

The shape index of the endothelial cells in the area of plaque growth of both models, with and without endothelial repair is represented in Figs. 8 and 9, respectively, for the case of update periods of the geometry and hemodynamic stimuli every 1.25 years. In Fig. 8 it can be observed that in the case of endothelial repair, the area of high SI changes longitudinally with every geometry update, while in Fig. 9 it can be seen that for the case without endothelial repair, different areas of high SI are accumulated.

Figs. 10 and 11 show the resultant geometries after 10 years of simulation for the cases with endothelial repair and without it. Additionally, the location of the maximum increase of the arterial wall thickness in each case is marked with a red dot, and its corresponding value is also included. As shown in Figs. 10 and 11, the position of the point of maximum increase of the wall thickness in both cases changes

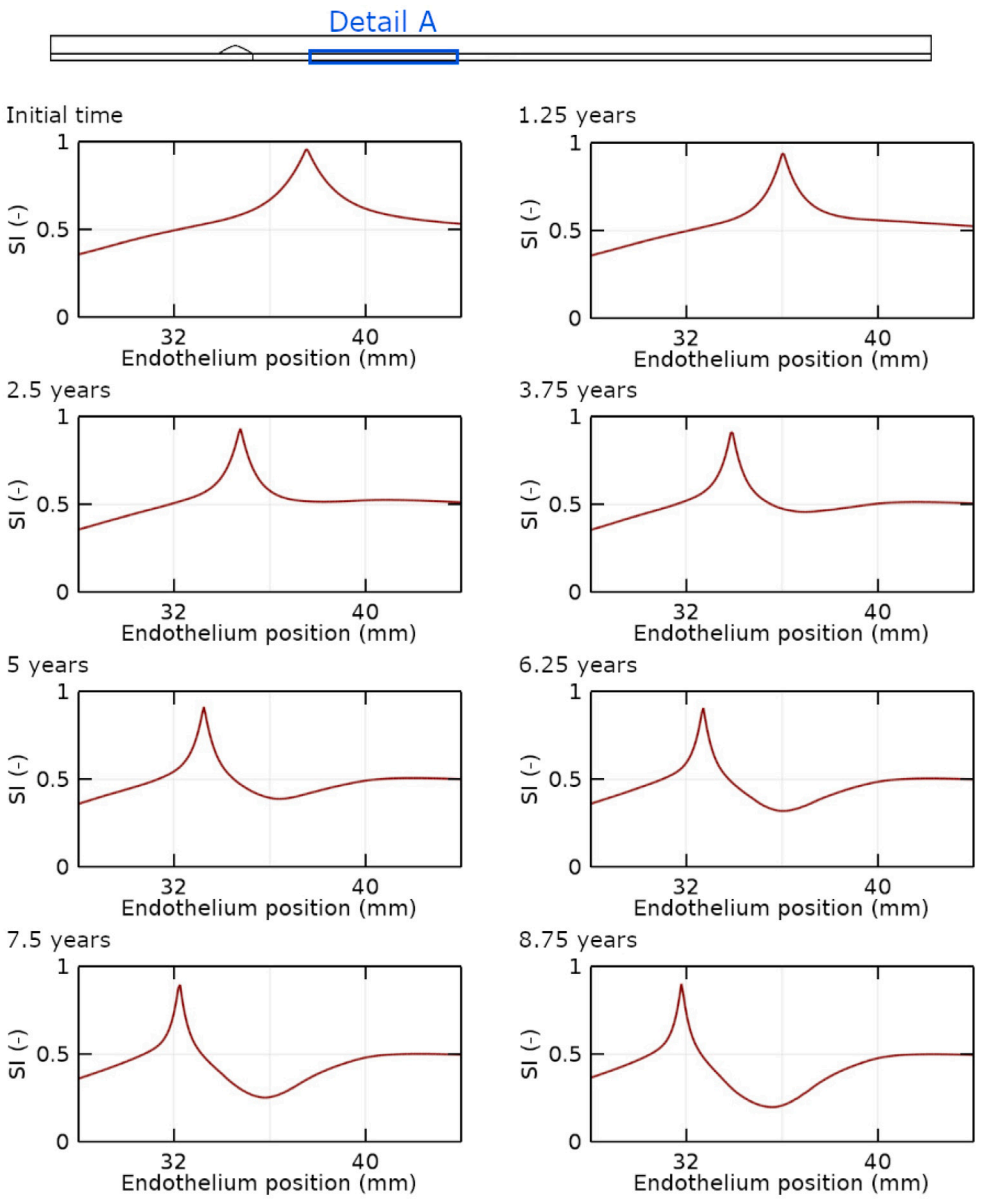

Fig. 8. Shape index of the endothelial cells in the area of plaque growth for all the time intervals of geometry updating every 1.25 years, for the case of FSI with endothelial repair.

over time, with a greater variation of the location in the case of the model with endothelial repair. In both cases (Figs. 10 and 11), the generated plaque has a more longitudinal and less radial shape than the plaque obtained with the uncoupled model. The maximum arterial wall thickness increase due to the plaque growth in the case with endothelial repair is equal to 0.35 mm, which corresponds to a 34.92% of stenosis ratio. In the case without endothelial repair, the maximum arterial wall thickness increase is 1.53 mm and corresponds to a 97.53% of stenosis ratio.

In Fig. 12 the concentration of the substances that contribute to the plaque volume are represented, for the simulation time of 10 years, in each one of the three computed models (the uncoupled model and the two models updating the geometry and hemodynamical stimuli). The change in the shape of the plaques already observed in Figs. 5, 10 and 11 can be noticed again. As visible, the highest concentration of FCs corresponds to the model without endothelial repair while the model with endothelial repair is the one with the lowest concentration of FCs. The distribution of SSMCs concentration is the same as the distribution of collagen fibers in all the analyzed models due to that the reactive terms of the collagen equation directly depend on the concentration of SSMCs. The highest concentration of SSMCs and collagen in year 10 can be found in the uncoupled model.

Fig. 13 shows the LDL concentration obtained for the three computed models after 10 years of simulation. As shown, due to the influence of the geometry and hemodynamics update, there are new plaques downstream of the analyzed ones. This is visible through the LDL accumulations in new areas of the arterial wall that is not existent in the uncoupled model. It is more marked in the case of the model which does not consider endothelial repair. It should be noted that atherosclerotic plaques are present in both scenarios (with and without endothelial repair). The arrows in Fig. 13 indicate the location of these plaques. In the case with endothelial repair, the plaque does not continue to grow and remains small because the endothelium repairs itself, reducing its permeability. In contrast, in the case without endothelial repair, the plaque continues to grow as the endothelium remains highly permeable, making the plaque more visible. We have added this explanation to the manuscript to better reflect the differences between the two scenarios.

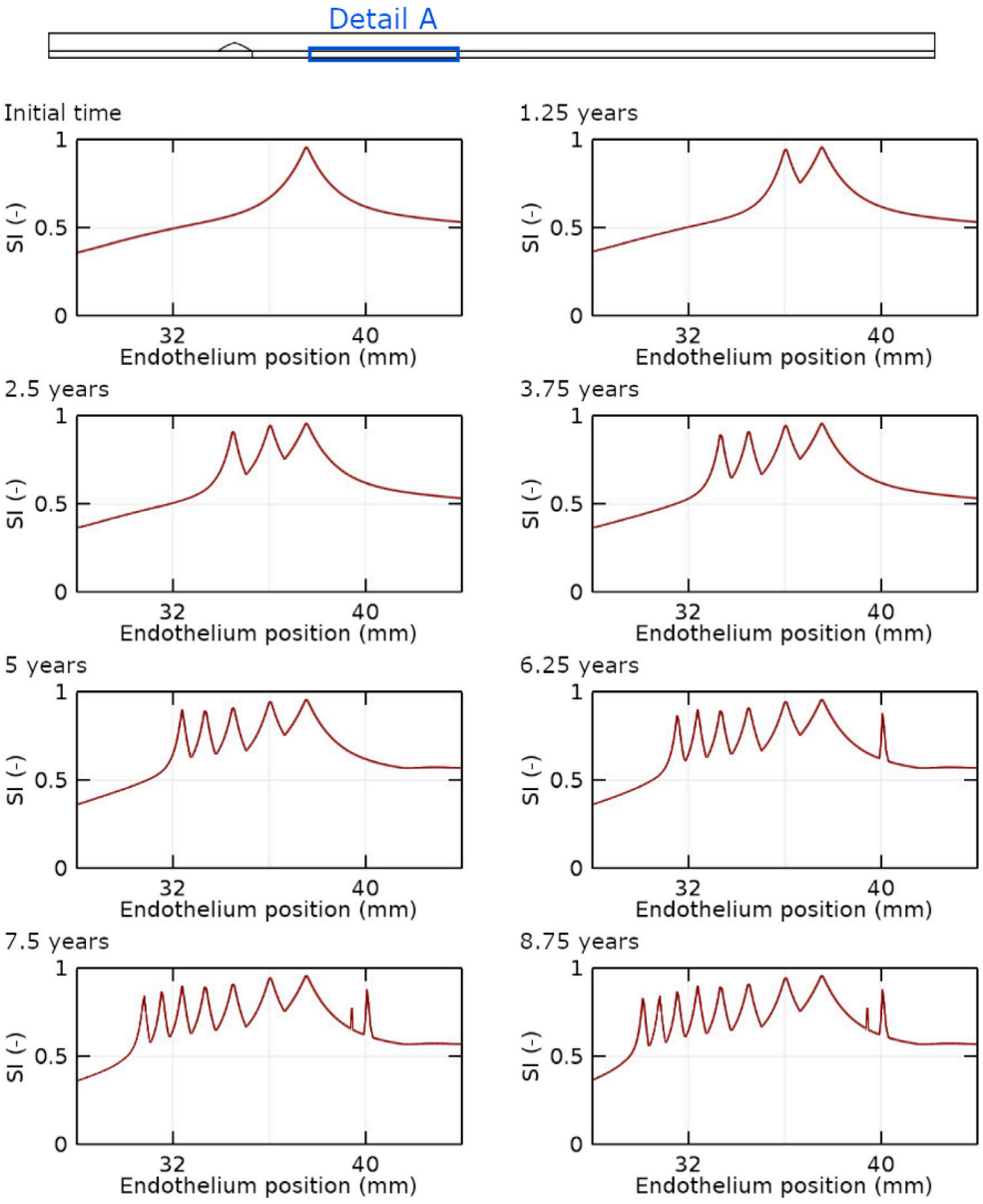

Fig. 9. Shape index of the endothelial cells in the area of plaque growth for all the time intervals of geometry updating every 1.25 years, for the case of FSI without endothelial repair.

4. Discussion

In this work, geometry and hemodynamical stimuli updates have been implemented improving a previously developed and validated model of atheroma plaque growth, used to computationally simulate pathology evolution in patient-specific geometries. The main objective of this study is to improve one of the limitations detected in that study [33]. Some real plaques were not accurately predicted by the computational model because it failed to account for geometric changes that influence hemodynamic alterations. Now, because the high computational costs of the patient-specific models, this improvement has been included in an axisymmetric model of a carotid artery. Although the model has been applied to a carotid artery geometry, it could be applied to other geometries or arteries adapting the corresponding parameters.

There are several computational models that consider FSI in atheroma plaques. Most of these models primarily focus on analyzing plaque stability based on the stresses induced by blood flow, as seen in the works of Tang et al. [28], Kock et al. [29] and Gao et al. [30], concluding that combining both plaque structural stress and flow shear stress gives better approximation results. However, there are also a few models that examine the influence of hemodynamic changes on atheroma plaque growth. For example, Calvez et al. [19] used a two-dimensional model with mesh displacement due to plaque formation. In addition, Chung and Vafai [31] investigated the effect of FSI on LDL flow across the endothelium and its accumulation in the arterial wall. Finally, Deyranlou et al. [32] investigated the impact of FSI on LDL accumulation, considering blood flow as a non-Newtonian fluid. To the best of the authors' knowledge, there are no existing models in the literature that combine detailed fluid dynamics and plaque growth processes involving as many substances as ours.

Due to the difference in time scales between the cardiac cycle and the inflammatory process of the arterial wall, a simplification has been done: the model with geometry updates has been calculated in a semi-coupled way. Given that the model was computed in a semi-coupled way, an analysis of the variation in results was conducted using geometry update intervals of 5, 2.5, and 1.25 years. Additionally, due to the behavior of the endothelial cells after changes in hemodynamics

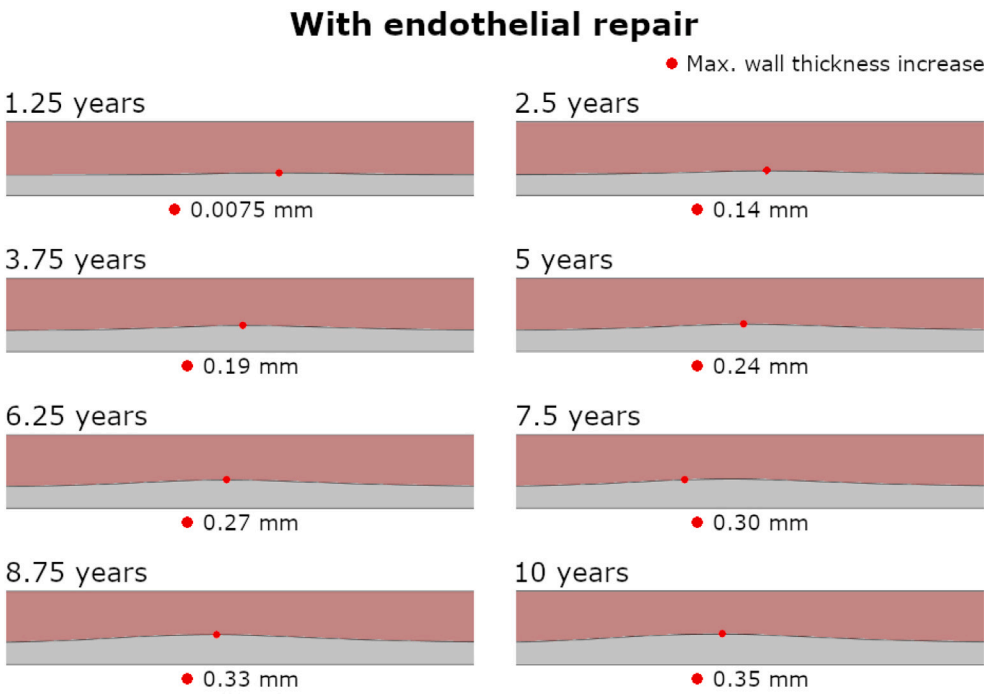

Fig. 10. Geometry and maximum wall thickness increase for all the time intervals of geometry updating every 1.25 years, for the case of FSI considering endothelial repair.

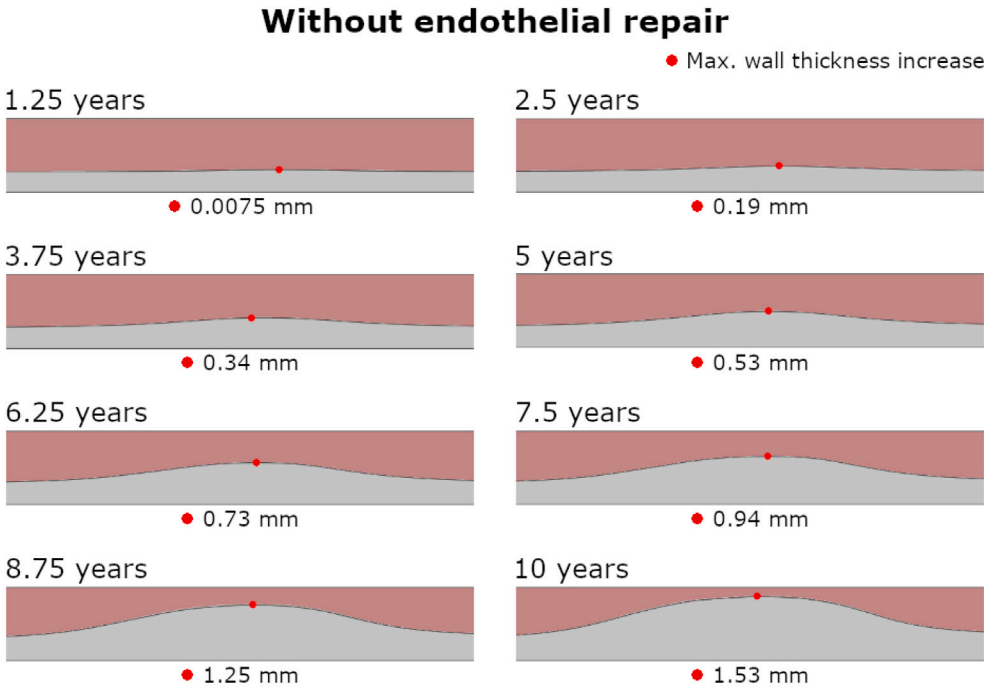

Fig. 11. Geometry and maximum wall thickness increase for all the time intervals of geometry updating every 1.25 years, for the case of FSI without considering endothelial repair.

is not completely known, two different models have been developed, considering the opposite cases of endothelial repair: The first one of these models considers endothelial repair when the hemodynamic stimuli change while, the second model, hypothesizes that once that the endothelial permeability increases, it remains elevated even if the hemodynamic stimulus that causes the increase changes and, therefore, no endothelial repair can be produced. In terms of convergence of results, it has been found that when endothelial repair is considered, this convergence is achieved for geometry update periods of 1.25 years. When endothelial repair is considered, the low WSS regions change gradually with each model update. The plaque grows during the specified time increment (1.25, 2.5 or 5 years) and starts to grow again in the new low WSS area after each update. More frequent updates limit the time available for plaque growth in each region, resulting in a smaller stenosis radius with more frequent updates, as shown in Fig. 4. In the case of the model without endothelial repair, such convergence is not achieved because as the update period decreases, more areas of substance flow through the endothelium appear, leading to more plaque growth, as shown in Fig. 5. In addition, for an update period of 1.25 years, a stenosis ratio close to 100% is obtained, while the

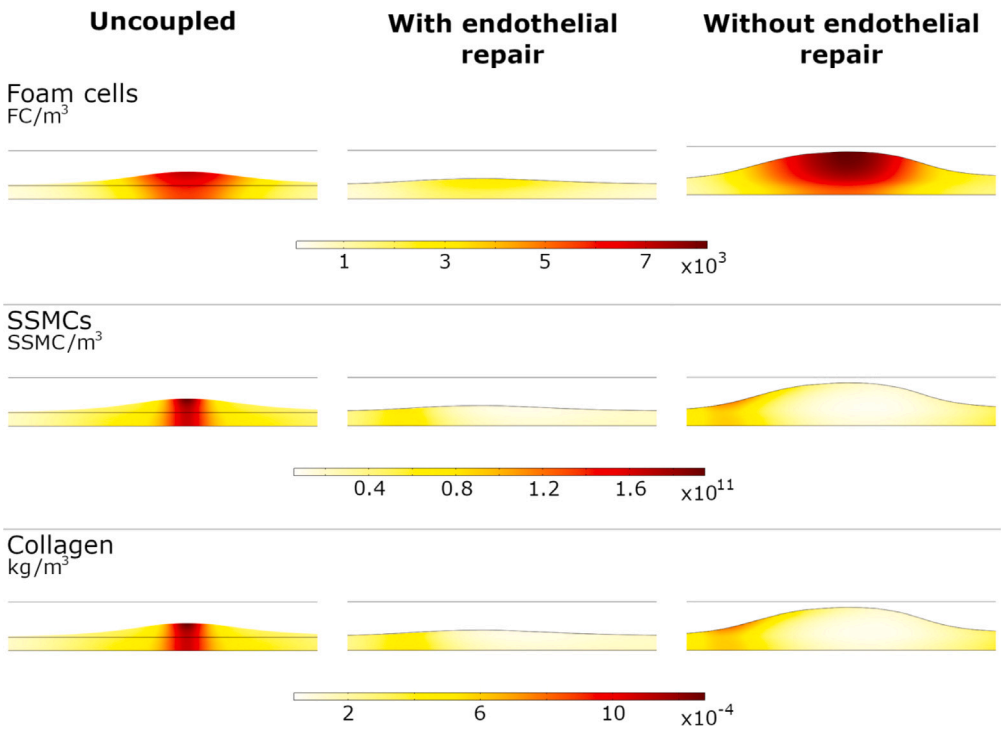

Fig. 12. Concentration of foam cells, SSMCs, and collagen after 10 years of simulation for the uncoupled model and the two models updating the geometry and hemodynamical stimuli.

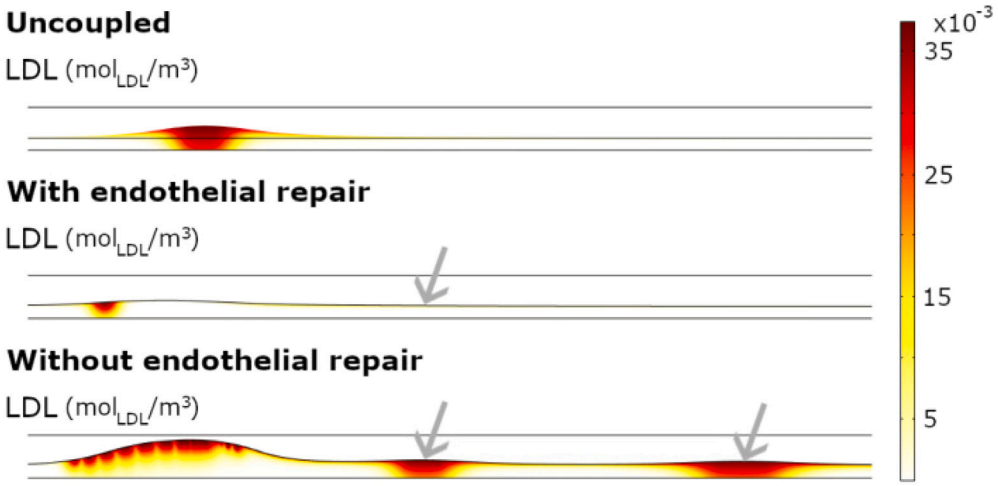

Fig. 13. LDL concentration after 10 years of simulation for the uncoupled model and the two models updating the geometry and hemodynamical stimuli.

plaque area continues to increase due to this phenomenon. In addition, the plaque growth obtained with the two models is different, which shows that the endothelial repair highly affects the global growth of the plaque.

Large differences are observed in the shape and the stenosis ratio of the plaques obtained with the uncoupled model and the two models with geometry and hemodynamic stimuli update. In the cases of the models considering geometry and hemodynamical changes, the new plaques extend more in longitudinal direction than the plaques obtained with the uncoupled model, as has been experimentally observed in clinical images of atheroma plaques [90,91]. Thus, geometrical and hemodynamics updates are two important elements to take into account in the process of atheroma plaque formation.

Of the three computed cases, the stenosis ratio and the plaque obtained for the case without endothelial repair is the highest, while that obtained in the case including endothelial repair is the smallest. This can be explained since in the case in which the endothelium is not repaired, the area of substances flowing through it is enlarged with each geometry update, while in the cases of endothelial repair, this area only changes, but does not increase its size. Therefore, in the case that considers endothelial repair, the substance flow area across the endothelium is higher than in the other two cases. This phenomenon, in addition, explains why the plaque is larger the more frequently the geometry is updated as there is a larger area of substances flow across the endothelium.

As it has been noticed, there is a change over time in the position of the maximum wall thickness increase point in the two models with geometrical updates. This change is due to the hemodynamic changes that lead to plaque growth in new areas. However, the displacement of this point is smaller in the model that does not consider endothelial repair. In fact, although there is a change in the hemodynamic stimuli,

the plaques continue growing in the areas with initial damaged endothelium. Thus, in the case without endothelial repair, the maximum increase in the arterial wall thickness will be located in the initial area of plaque growth because of the formation of the atheroma plaque.

On the other hand, the highest concentration of FCs corresponds to the model without endothelial repair because, as mentioned, the accumulation of areas of substance flow from the lumen into the arterial wall. For the same reason, the model that considers endothelial repair is the model with the lowest FCs concentration.

Furthermore, it has been observed that, in both models with geometrical updates, some new plaques naturally grow downstream of the first one. This phenomenon has been observed in clinical practice [35,36]. However, these new plaques do not appear in the case of the uncoupled model, as in that case, the formation of a plaque does not disturb blood flow downstream it.

While this study presents a generalized computational framework for atheroma plaque growth, it is important to consider the potential for applying this model to animal and patient-specific cases. For validation purposes, our model has already been tested on human patient-specific geometries [33]. Tailoring the model to individual cases would allow for a more accurate representation of specific geometries, hemodynamics and biological responses. Such adaptations could significantly improve the predictive power of the model and aid in the early detection and personalized treatment of atherosclerosis. Using imaging data such as MRI, CT or ultrasound, it is possible to reconstruct the arterial geometry and implement personalized boundary conditions based on the patient's blood flow and pressure measurements. This would allow clinicians to predict disease progression and evaluate the efficacy of different treatment strategies adapted to the individual patient. Finally, the computational model has some limitations, as it only considers the main substances involved in the atherosclerosis process and does not consider, for example, high-density lipoproteins, oxygen or metalloproteinases, or free radicals that oxidize LDL. Only the primary processes were included, and other important factors in atheroma plaque development, such as collagen degradation with age, were not considered. Hemodynamics was treated as the main trigger for the initiation of atherosclerosis, thus the effects of cyclic stretching due to vessel compliance or curvature were not considered, as the model is 2D. Another limitation of our model is the lack of real patient geometries. Therefore, from the results obtained and despite the limitations of the model, it can be concluded that hemodynamical changes due to atheroma plaque growth have a major influence on the process of atheroma plaque formation and should not be neglected. As one of the main drawbacks of the study, the model has high computational costs and requires very long computational time. This necessary time varies depending on the model and the update period for the plaque growth at each geometry update. For example, in the case of the model that does not consider endothelial repair, the calculation time was more than 8 days for the last geometry update with periods of 1.25 years (calculated with an Intel(R) Core(TM) i7-6700CPU; 3.40 GHz; 4 cores). Therefore, it is hardly feasible to apply it to the 3D complex models. A fully coupled model is very demanding. Ideally, the best update interval would coincide with a fully coupled model.

CRediT authorship contribution statement

Patricia Hernández-López: Writing – review & editing, Writing – original draft, Methodology, Formal analysis. **Myriam Cilla:** Writing – review & editing, Formal analysis. **Miguel A. Martínez:** Writing – review & editing, Funding acquisition, Formal analysis, Conceptualization. **Estefanía Peña:** Writing – review & editing, Funding acquisition, Formal analysis, Conceptualization. **Mauro Malvè:** Writing – review & editing, Formal analysis, Conceptualization.

Declaration of competing interest

The authors declare that they have no known competing financial interests or personal relationships that could have appeared to influence the work reported in this paper.

Acknowledgments

The authors thank the research support from the CIBER initiative, whose actions are financed by the Instituto de Salud Carlos III with assistance from the European Regional Development Fund.

Funding

Support was obtained from the Spanish Ministry of Science and Technology through the research projects PID2019-107517RB-I00 and PID2022-140219OB-I00 and financial support to P. Hernández-López from the grant BES-2017-080239, and the regional Government of Aragón support for the funding of the research project T24-20R. Myriam Cilla is supported by Grant Ramón y Cajal grant 171562 funded by MICIU/AEI/ 10.13039/501100011033 and the European Social Fund Plus (FSE+). M. Malvè is supported by grant PID2021-125731OB-C31 from the Spanish Ministry of Science and Innovation MCIN/AEI/10.13039/501100011033/ and Fondo Europeo de Desarrollo Regional (FEDER) ("A way to build Europe").

References

[1] J.D. Humphrey, Cardiovascular Solid Mechanics: Cells, Tissues and Organs, Springer-Verlag, New York, 2002.
[2] World Health Organisation, 2019, https://www.who.int/news-room/fact-sheets/detail/the-top-10-causes-of-death.
[3] J. Stamler, O. Vaccaro, J. Neaton, D. Wentworth, Diabetes, other risk factors, and 12-yr cardiovascular mortality for men screened in the multiple risk factor intervention trial, Diabetes Care 16 (1993) 434–444.
[4] P., L., Inflammation in atherosclerosis, Nature 420 (2002) 868–874.
[5] Y. Chatzizisis, A. Coskun, M. Jonas, E. Edelman, C. Feldman, P. Stone, Role of endothelial shear stress in the natural history of coronary atherosclerosis and vascular remodeling: molecular, cellular, and vascular behavior, J. Am. College Cardiol. 49 (2007) 2379–2393.
[6] D. Steinberg, J.C. Khoo, C.K. Glass, W. Palinski, F. Almazan, A new approach to determining the rates of recruitment of circulating leukocytes into tissues: Application to the measurement of leukocyte recruitment into atherosclerotic lesions, Proc. Natl. Acad. Sci. USA 94 (1997) 4040–4044, http://dx.doi.org/10.1073/pnas.94.8.4040.
[7] B. Zhao, Y. Li, C. Buono, S.W. Waldo, N.L. Jones, M. Mori, H.S. Kruth, Constitutive receptor-independent low density lipoprotein uptake and cholesterol accumulation by macrophages differentiated from human monocytes with macrophage-colony-stimulating factor (m-csf), J. Biol. Chem. 281 (2006) 15757–15762, http://dx.doi.org/10.1074/jbc.M510714200.
[8] S. Howarth, Z.Y. Li, R. Trivedi, J. U-King-Im, M. Graves, P. Kirkpatrick, J. Gillard, Correlation of macrophage location and plaque stress distribution using uspio-enhanced mri in a patient with symptomatic severe carotid stenosis: a new insight into risk stratification, Br. J. Neurosurg. 21 (2007) 396–398.
[9] G. Holzapfel, J. Mulvihill, E. Cunnane, M. Walsh, Computational approaches for analyzing the mechanics of atherosclerotic plaques: a review, J. Biomech. 47 (2014) 859–869.
[10] G. Di Tomaso, V. Díaz-Zuccarini, C., P.A., A multiscale model of atherosclerotic plaque formation at its early stage, IEEE Trans. Biomed. Eng. 58 (2011) 3460–3463.
[11] S. Chung, K. Vafai, Effect of the fluid–structure interactions on low density lipoprotein transport within a multi-layered arterial wall, J. Biomech. 45 (2012) 371–381.
[12] S. Chung, K. Vafai, Low-density lipoprotein transport within a multi-layered arterial wall-effect of the atherosclerotic plaque/stenosis, J. Biomech. 46 (2013) 574–585.
[13] A. Parton, V. McGilligan, M. O'Kane, F. Baldrick, S. Watterson, Computational modelling of atherosclerosis, briefings in bioinformatics, Briefings Bioinform. 17 (2016) 562–575.
[14] T. Zohdi, A. olzapfel, S. Berger, A phenomenological model for atherosclerotic plaque growth and rupture, J. Theoret. Biol. 227 (2004) 437–443.
[15] C. Cobbold, J. Sherratt, S. Maxwell, Lipoprotein oxidation and its significance for atherosclerosis: a mathematical approach, Bull. Math. Biol. 64 (2002) 65–95.

[16] V. Gessaghi, M. Raschi, D. Tanoni, C. Perazzo, A. Larreteguy, Growth model for cholesterol accumulation in the wall of a simplified 3d geometry of the carotid bifurcation, Comput. Methods Appl. Mech. Engrg. 200 (2011) 2117–2125.
[17] P.W. Fok, Mathematical model of intimal thickening in atherosclerosis: Vessel stenosis as a free boundary problem, J. Theoret. Biol. 314 (2002) 23–33, http://dx.doi.org/10.1016/j.jtbi.2012.07.029.
[18] P. Siogkas, A. Sakellarios, T. Exarchos, L., A., E. Karvounis, K. Stefanou, D. Fotiou, K. Naka, L. Michalis, N. Filipovic, O., P., Multiscale-patient-specific artery and atherogenesis models, IEEE Trans. Biomed. Eng. 58 (2011) 3464–3468.
[19] V. Calvez, A. Ebde, N. Meunier, A. Raoult, Mathematical modelling of the atherosclerotic plaque formation, in: European Series in Applied and Industrial Mathematics: Proceedings, 28, 2009, pp. 1–12, http://dx.doi.org/10.1051/proc/2009036.
[20] O. Ogunrinade, G.T. Kameya, G.A. Truskey, Effect of fluid shear stress on the permeability of the arterial entohelium, Ann. Biomed. Eng. 30 (2002) 430–446, http://dx.doi.org/10.1114/1.1467924.
[21] M.A.K. Bulelzai, J.L.A. Dubbeldam, Long time evolution of atherosclerotic plaques, J. Theoret. Biol. 297 (2012) 1–10, http://dx.doi.org/10.1016/j.jtbi.2011.11.023.
[22] A. Corti, C. Chiastra, M. Colombo, M. Garbey, F. Migliavacca, S. Casarin, A fully coupled computational fluid dynamics – agent-based model of atherosclerotic plaque development: Multiscale modeling framework and parameter sensitivity analysis, Comput. Biol. Med. 118 (2020) 103623.
[23] A. Corti, M. Colombo, F. Migliavacca, J.F., R.M., S. Casarin, C. Chiastra, Multiscale computational modeling of vascular adaptation: A systems biology approach using agent-based models, Front. Bioeng. Biotechnol. 9 (2021) 744560.
[24] P. Zun, T. Anikina, A. Svitenkov, A.G, H, A comparison of fully-coupled 3d in-stent restenosis simulations to in-vivo data, Front. Physiol. 8 (2017) 1–12.
[25] C. Boyle, A. Lennon, M. Early, D. Kelly, C. Lally, P. Prendergast, Computational simulation methodologies for mechanobiological modelling: a cell-centred approach to neointima development in stents, Philos. Trans.: Math. Phys. Eng. Sci. 368 (2010) 2919–2935.
[26] D. Lopes, H. Puga, J. Teixeira, R. Lima, Blood flow simulations in patient-specific geometries of the carotid artery: A systematic review, J. Biomech. 111 (2020) 110019.
[27] M. Hirschhorn, V. Tchantchaleishvili, R. Stevens, J. Rossano, A. Throckmorton, Fluid–structure interaction modeling in cardiovascular medicine - a systematic review, Med. Eng. Phys. 78 (2020) 1–13.
[28] D. Tang, C. Yang, S. Mondal, F. Liu, G. Canton, T.S. Hatsukami, C. Yuan, A negative correlation between human carotid atherosclerotic plaque progression and plaque wall stress: In vivo mri-based 2d/3d fsi models, J. Biomech. 41 (2008) 727–736, http://dx.doi.org/10.1016/j.jbiomech.2007.11.026.
[29] S.A. Kock, J.V. Nygaard, N. Eldrup, E.T. Früand, A. Klæ rke, W.P. Paaske, E. Falk, K.W. Yong, Mechanical stresses in carotid plaques using mri-based fluid–structure interaction models, J. Biomech. 41 (2008) 1651–1658, http://dx.doi.org/10.1016/j.jbiomech.2008.03.019.
[30] H. Gao, Q. Long, M. Graves, J.H. Gillard, Z.Y. Li, Carotid arterial plaque stress analysis using fluid–structure interactive simulation based on in-vivo magnetic resonance images of four patients, J. Biomech. 42 (2009) 1416–1423, http://dx.doi.org/10.1016/j.jbiomech.2009.04.010.
[31] S. Chung, K. Vafai, Effect of the fluid–structure interactions on low-density lipoprotein transport within a multi-layered arterial wall, J. Biomech. 45 (2012) 371–381, http://dx.doi.org/10.1016/j.jbiomech.2011.10.002.
[32] A. Deyranlou, H. Niazmand, M.R. Sadeghi, Low-density lipoprotein accumulation within a carotid artery with multilayer elastic porous wall: Fluid–structure interaction and non-newtonian considerations, J. Biomech. 48 (2015) 2948–2959, http://dx.doi.org/10.1016/j.jbiomech.2015.08.002.
[33] P. Hernández-López, M. Cilla, M.A. Martínez, E. Peña, Effects of the haemodynamic stimulus on the location of carotid plaques based on a patient-specific mechanobiological plaque atheroma formation model, Front. Bioeng. Biotechnol. 9 (2021) 690685, http://dx.doi.org/10.3389/fbioe.2021.690685, https://www.frontiersin.org/articles/10.3389/fbioe.2021.690685.
[34] P. Hernández-López, M.A. Martínez, E. Peña, M. Cilla, Understanding the parameter influence on lesion growth for a mechanobiology model of atherosclerosis, Mathematics 11 (2023) 829, http://dx.doi.org/10.3390/math11040829, https://www.mdpi.com/2227-7390/11/4/829.
[35] B. De Bruyne, N.H.J. Pijls, G.R. Heyndrickx, D. Hodeige, R.L. Kirkeeide, K.L. Gould, Pressure-derived fractional flow reserve to assess serial epicardial stenoses: theoretical basis and animal validation, Circulation 101 (2000) 1840–1847, http://dx.doi.org/10.1161/01.cir.101.15.1840.
[36] N.H.J. Pijls, B. De Bruyne, G.J.W. Bech, F. Liistro, G.R. Heyndrickx, J.J.R.M. Bonnier, J.J. Koolen, Coronary pressure measurement to assess the hemodynamic significance of serial stenosis within one coronary-artery: validation in humans, Circulation 102 (2000) 2371–2377, http://dx.doi.org/10.1161/01.cir.102.19.2371.
[37] C. Caro, T. Pedley, R. Schroter, W. Seed, The Mechanics of the Circulation, Oxford University Press, Oxford, 1978.
[38] K. Perktold, M. Resch, H. Florian, Pulsatile non-newtonian flow characteristics in a three-dimensional human carotid bifurcation model, J. Biomech. Eng. 113 (1991) 464–475, http://dx.doi.org/10.1115/1.2895428.
[39] M. Malvè, S. Chandra, A. García, A. Mena, M.A. Martínez, E.A. Finol, M. Doblaré, Impedance-based outflow boundary conditions for human carotid haemodynamics, Comput. Methods Biomech. Biomed. Eng. 17 (2014) 1248–1260, http://dx.doi.org/10.1080/10255842.2012.744396.
[40] W.R. Milnor, Hemodynamics, second ed., Williams and Wilkins, Baltimore, MD, 1989.
[41] M. Cilla, Mechanical Effects on the Atheroma Plaque Appearance, Growth and Vulnerability (Ph.D. Thesis), University of Zaragoza, Spain, 2013.
[42] F.E. Curry, A hydrodynamic description of the osmotic reflection coefficient with application to the pore theory of transcapillary exchange, Microvasc. Res. 8 (1974) 236–252, http://dx.doi.org/10.1016/0026-2862(74)90097-1.
[43] O. Kedem, A. Katchalsky, Thermodynamic analysis of the permeability of biological membranes to non-electrolytes, Biochim. Biophys. Acta 27 (1958) 229–246, http://dx.doi.org/10.1016/0006-3002(58)90330-5.
[44] U. Olgac, V. Kurtcuoglu, D. Poulikakos, Computational modeling of coupled blood-wall mass transport of LDL: Effects of local wall shear stress, Am. J. Physiol. - Heart Circ. Physiol. 294 (2008) 909–919, http://dx.doi.org/10.1152/ajpheart.01082.2007.
[45] A. Tedgui, M.J. Lever, Filtration through damaged and undamaged rabbit thoracic aorta, Am. J. Physiol.-Heart Circ. Physiol. 247 (1984) H784–H791, http://dx.doi.org/10.1152/ajpheart.1984.247.5.H784.
[46] S. Weinbaum, G. Tzeghai, P. Ganatos, R. Pfeffer, S. Chien, Effect of cell turnover and leaky junctions on arterial macromolecular transport, Am. J. Physiol.-Heart Circ. Physiol. 248 (1985) H945–H960, http://dx.doi.org/10.1152/ajpheart.1985.248.6.H945.
[47] Y. Huang, D. Rumschitzki, S. Chien, S. Weinbaum, A fiber matrix model for the growth of macromolecular leakage spots in the arterial intima, J. Biomech. Eng. 116 (1994) 430–445, http://dx.doi.org/10.1115/1.2895794.
[48] Z.J. Huang, J.M. Tarbell, Numerical simulation of mass transfer in porous media of blood vessel walls, Am. J. Physiol.-Heart Circ. Physiol. 273 (1997) H464–H477, http://dx.doi.org/10.1152/ajpheart.1997.273.1.h464.
[49] N. Filipovic, Z. Teng, M. Radovic, I. Saveljic, D. Fotiadis, O. Parodi, Computer simulation of three-dimensional plaque formation and progression in the carotid artery, Med. Biol. Eng. Comput. 51 (2013) 607–616, http://dx.doi.org/10.1007/s11517-012-1031-4.
[50] S.Z. Zhao, B. Ariff, Q. Long, A.D. Hughes, S.A. Thom, A.V. Stanton, X.Y. Xu, Inter-individual variations in wall shear stress and mechanical stress distributions at the carotid artery bifurcation of healthy humans, J. Biomech. 35 (2002) 1367–1377, http://dx.doi.org/10.1016/S0021-9290(02)00185-9.
[51] H.F. Younis, M.R. Kaazempur-Mofrad, R.C. Chan, A.G. Isasi, D.P. Hinton, A.H. Chau, L.A. Kim, R.D. Kamm, Hemodynamics and wall mechanics in human carotid bifurcation and its consequences for atherogenesis: Investigation of inter-individual variation, Biomech. Model. Mechanobiol. 3 (2004) 17–32, http://dx.doi.org/10.1007/s10237-004-0046-7.
[52] S. Chien, Molecular and mechanical bases of focal lipid accumulation in arterial wall, Prog. Biophys. Mol. Biol. 83 (2003) 131–151, http://dx.doi.org/10.1016/S0079-6107(03)00053-1.
[53] S.J. Lin, K.M. Jan, S. Weinbaum, S. Chien, Transendothelial transport of low density lipoprotein in association with cell mitosis in rat aorta, Arteriosclerosis 9 (1989) 230–236, http://dx.doi.org/10.1161/01.atv.9.2.230.
[54] F. Yuan, S. Chien, S. Weinbaum, A new view of convective-diffusive transport processes in the arterial intima, J. Biomech. Eng. 113 (1991) 314–329, http://dx.doi.org/10.1115/1.2894890.
[55] M. Prosi, P. Zunino, K. Perktold, A. Quarteroni, Mathematical and numerical models for transfer of low-density lipoproteins through the arterial walls: A new methodology for the model set up with applications to the study of disturbed lumenal flow, J. Biomech. 38 (2005) 903–917, http://dx.doi.org/10.1016/j.jbiomech.2004.04.024.
[56] L. Ai, K. Vafai, A coupling model for macromolecule transport in a stenosed arterial wall, Int. J. Heat Mass Transfer 49 (2006) 1568–1591, http://dx.doi.org/10.1016/j.ijheatmasstransfer.2005.10.041.
[57] J.M. Tarbell, Mass transport in arteries and the localization of atherosclerosis, Annu. Rev. Biomed. Eng. 5 (2003) 79–118, http://dx.doi.org/10.1146/annurev.bioeng.5.040202.121529.
[58] M. Cilla, E. Peña, M.A. Martínez, Mathematical modelling of atheroma plaque formation and development in coronary arteries, J. R. Soc. Interface 11 (2013) 20130866, http://dx.doi.org/10.1098/rsif.2013.0866.
[59] L.M. Cancel, A. Fitting, J.M. Tarbell, In vitro study of LDL transport under pressurized (convective) conditions, Am. J. Physiol. - Heart Circ. Physiol. 293 (2007) 126–132, http://dx.doi.org/10.1152/ajpheart.01188.2006.
[60] C.S. Patlak, D.A. Goldstein, J.F. Hoffman, The flow of solute and solvent across a two-membrane system, J. Theoret. Biol. 5 (1963) 426–442, http://dx.doi.org/10.1016/0022-5193(63)90088-2.
[61] E.M. Renkin, Filtration, diffusion, and molecular sieving through porous cellulose membranes, J. Gen. Physiol. 38 (1954) 225–243.
[62] F.H. Khan, The Elements of Immunology, Pearson Education, India, 2009.
[63] N. Sun, N.B. Wood, A.D. Hughes, S.A.M. Thom, X.Y. Xu, Effects of transmural pressure and wall shear stress on LDL accumulation in the arterial wall: A numerical study using a multilayered model, Am. J. Physiol. - Heart Circ. Physiol. 292 (2007) 3148–3157, http://dx.doi.org/10.1152/ajpheart.01281.2006.

[64] M. Dabagh, P. Jalali, J.M. Tarbell, The transport of LDL across the deformable arterial wall: The effect of endothelial cell turnover and intimal deformation under hypertension, Am. J. Physiol. - Heart Circ. Physiol. 297 (2009) 983–996, http://dx.doi.org/10.1152/ajpheart.00324.2009.

[65] G. Meyer, R. Merval, A. Tedgui, Effects of pressure-induced stretch and convection on low-density lipoprotein and albumin uptake in the rabbit aortic wall, Circ. Res. 79 (1996) 532–540, http://dx.doi.org/10.1161/01.RES.79.3.532.

[66] E.A. Ivanova, V.A. Myasoedova, A.A. Melnichenko, A.V. Grechko, A.N. Orekhov, Small dense low-density lipoprotein as biomarker for atherosclerotic diseases, Oxid. Med. Cell. Longevity 2017 (2017) 1273042, http://dx.doi.org/10.1155/2017/1273042.

[67] J. Escuer, M.A. Martínez, S. McGinty, E. Peña, Mathematical modelling of the restenosis process after stent implantation, J. R. Soc. Interface 16 (2019) 20190313, http://dx.doi.org/10.1098/rsif.2019.0313.

[68] R.E. Tracy, Declining density of intimal smooth muscle cells as a precondition for atheronecrosis in the coronary artery, Virchows Archiv: Eur. J. Pathol. 430 (1997) 155–162, http://dx.doi.org/10.1007/BF01008037.

[69] W. Zhao, C.A. Oskeritzian, A.L. Pozez, L.B. Schwartz, Cytokine production by skin-derived mast cells: Endogenous proteases are responsible for degradation of cytokines, J. Immunol. 175 (2005) 2635–2642, http://dx.doi.org/10.4049/jimmunol.175.4.2635.

[70] H. Zahedmanesh, H. Van Oosterwyck, C. Lally, A multi-scale mechanobiological model of in-stent restenosis: deciphering the role of matrix metalloproteinase and extracellular matrix changes, Comput. Methods Biomech. Biomed. Eng. 17 (2014) 813–828, http://dx.doi.org/10.1080/10255842.2012.716830.

[71] R.V. Krstic, Human Microscopic Anatomy: An Atlas for Students of Medicine and Biology, Springer, Berlin, Germany, 1997.

[72] G.J. Cannon, J.A. Swanson, The macrophage capacity for phagocytosis, J. Cell Sci. 101 (1992) 907–913, http://dx.doi.org/10.1242/jcs.101.4.907.

[73] C.J. Boyle, A.B. Lennon, P.J. Prendergast, In silico prediction of the mechanobiological response of arterial tissue: Application to angioplasty and stenting, J. Biomech. Eng. 133 (2011) 1–10, http://dx.doi.org/10.1115/1.4004492.

[74] M.R. Bennett, G.I. Evan, S.M. Schwartz, Apoptosis of human vascular smooth muscle cells derived from normal vessels and coronary atherosclerotic plaques, J. Clin. Investig. 95 (1995) 2266–2274, http://dx.doi.org/10.1172/JCI117917.

[75] O.H. Yeoh, Some forms of the strain energy function for rubber, Rubber Chem. Technol. 66 (1993) 754–771, http://dx.doi.org/10.5254/1.3538343.

[76] D.R. Nolan, J.P. McGarry, On the compressibility of arterial tissue, Ann. Biomed. Eng. 44 (2016) 993–1007, http://dx.doi.org/10.1007/s10439-015-1417-1.

[77] C. Westhorpe, E. Dufour, A. Maisa, A. Jaworowski, S. Crowe, W. Muller, Endothelial cell activation promotes foam cell formation by monocytes following transendothelial migration in an in vitro model, Exp. Mol. Pathol. 93 (2012) 220–226.

[78] A. Nakano, M., M., J. Seki, The three-dimensional structure of vascular smooth muscle cells: a confocal laser microscopic study of rabbit mesenteric arterioles, Asian Biomed. 1 (2010) 77–86.

[79] F. Krombach, S. Münzing, A.M. Allmeling, J.T. Gerlach, J. Behr, M. Dörger, Cell size of alveolar macrophagues: an interspecies comparison, Environ. Health Perspect. 105 (1997) 1261–1263, http://dx.doi.org/10.1289/ehp.97105s51261.

[80] P. Sáez, E. Peña, M.A. Martínez, E. Kuhl, Mathematical modeling of collagen turnover in biological tissue, J. Math. Biol. 67 (2013) 1765–1793, http://dx.doi.org/10.1007/s00285-012-0613-y.

[81] H.A. Himburg, D.M. Grzybowski, A.L. Hazel, J.A. LaMack, X. Li, M.H. Friedman, Spatial comparison between wall shear stress measures and porcine arterial endothelial permeability, Am. J. Physiol.-Heart Circ. Physiol. 286 (2004) H1916–H1922, http://dx.doi.org/10.1152/ajpheart.00897.2003.

[82] K.S. Cunningham, A.I. Gotlieb, The role of shear stress in the pathogenesis of atherosclerosis, Laboratory Investig. 85 (2005) 9–23, http://dx.doi.org/10.1038/labinvest.3700215.

[83] B.L. Langille, J.J. Graham, D. Kim, A.I. Gotlieb, Dynamics of shear-induced redistribution of f-actin in endothelial cells in vivo, Arteriosclerosis Thrombosis: J. Vasc. Biol. 11 (1991) 1814–1820, http://dx.doi.org/10.1161/01.ATV.11.6.1814.

[84] J.S. VanEpps, D.A. Vorp, Mechanopathobiology of atherogenesis: A review, J. Surgical Res. 142 (2007) 202–2017, http://dx.doi.org/10.1016/j.jss.2006.11.001.

[85] C.J. Slager, J.J. Wentzel, F.J.H. Gijsen, J.C.H. Schuurbiers, A.C. van der Wal, A.F.W. van der Steen, P.W. Serruys, The role of shear stress in the generation of rupture-prone vulnerable plaques, Nat. Clin. Pract. Cardiovasc. Med. 2 (2005) 401–407, http://dx.doi.org/10.1038/ncpcardio0274.

[86] K.F. Bürrig, The endothelium of advanced arteriosclerotic plaques in humans, Arteriosclerosis Thrombosis: J. Vascular Biol. 11 (1991) 1678–1689, http://dx.doi.org/10.1161/01.ATV.11.6.1678.

[87] O. Tricot, Z. Mallat, C. Heymes, J. Belmin, G. Lesèche, A. Tedgui, Relation between endothelial cell apoptosis and blood flow direction in human atherosclerotic plaques, Circulation 101 (2000) 2450–2453, http://dx.doi.org/10.1161/01.CIR.101.21.2450.

[88] Project-PARASOL, CERFACs, IRIT-ENSEEIHT, and RAL. Multi-frontal massively parallel sparse direct solver, MUMPS, 1999, https://mumps-solver.org.

[89] C.F. Curtiss, J.O. Hirschfelder, Integration of stiff equations, Proc. Natl. Acad. Sci. 38 (1952) 235–243, http://dx.doi.org/10.1073/pnas.38.3.235.

[90] A. Soloperto, N.G. Keenan, M.N. Sheppard, J. Ohayon, N.B. Wood, D.J. Pennell, R.H. Mohiaddin, X.Y. Xu, Combined imaging, computational and histological analysis of a ruptured carotid plaque: A patient-specific analysis, Artery Res. 4 (2010) 59–65, http://dx.doi.org/10.1016/j.artres.2010.05.001.

[91] J.R. Leach, V.L. Rayz, B. Soares, M. Wintermark, M.R. Mofrad, D. Saloner, Carotid atheroma rupture observed in vivo and FSI-predicted stress distribution based on pre-rupture imaging, Ann. Biomed. Eng. 38 (2010) 2748–2765, http://dx.doi.org/10.1007/s10439-010-0004-8.